Interim Report

Project UXO-1387

"Seismic Imaging of UXO-Contaminated Underwater Sites"

Roland Gritto[1,2], Valeri Korneev[1], Kurt Nihei[1], Lane Johnson[1]

[1]Lawrence Berkeley National Laboratory
and
[2]University of California Berkeley
Department of Environmental Sciences and Engineering

Summary

Finite difference modeling with 2-dimensional models were conducted to evaluate the performance of source-receiver arrays to locate UXO in littoral environments. The model parameters were taken from measurements in coastal areas with typical bay mud and from examples in the literature. Seismic arrays are well suited to focus energy by steering the elements of the array to any point in the medium that acts as an energy source. This principle also applies to seismic waves that are backscattered by buried UXO. The power of the array is particularly evident in strong noise conditions when the signal-to-noise ratio is too low to observe the scattered signal on the seismograms. Using a seismic array, it was possible to detect and locate the UXO with a reliability similar to noise free situations. When the UXO was positioned within 3-6 wavelengths of the incident signal from the source array, the resolution was good enough to determine the dimensions of the UXO from the scattered waves. Beyond this distance this distinction decreased gradually while the location and the center of the UXO were still determined reliably. The location and the dimensions of two adjacent UXO were resolved down to a separation of 1/3 of the dominant wavelength of the incident wave, at which time interference effects began to appear. In the investigated cases, the ability to locate a UXO was independent on the use of a model with a rippled or a flat seafloor, as long as the array was located above the UXO. Nevertheless, the correct parameters of the seafloor interface were obtained in these cases. An investigation to find the correct migration velocity in the sediments to locate the UXO revealed that a range of velocity gradients centered around the correct velocity model produced comparable results, which needs to be further investigated with physical modeling.

Introduction

In recent years, the evolution in hydrocarbon exploration from two- to three-dimensional seismic methods has resulted in improved resolution and better definition of the subsurface geological structure and prospects. These methods were developed to overcome the complicated structure of some areas where tectonic features (i.e., faults, fractures, salt domes) adversely affect seismic wave propagation through strong scattering and attenuation. Although the homogeneity of the media and the geometry of the experiment involved in marine unexploded ordnance (UXO) detection is relatively simple compared to the complexity of geologic earth models, the marine environment still comprises some degree of complexity considering the short wavelength of the seismic waves needed to yield sufficient resolution. The rugosity of the sea floor determines the coupling and the coherency of the seismic wavefield as it propagates into and out of the sediments, and therefore, the signal-to-noise ratio of the backscattered energy by the UXO. However, seafloor rugosity can scatter coherent energy into the sediments at angles larger than the critical angle. Biologic activity in the upper parts of the sediments may cause anaerobic conditions producing gas pockets that attenuate the seismic signal and constrain the maximum penetration of the waves. If free gas is present in the sediments, it may produce anelastic attenuation particularly for the shorter wavelengths of the seismic signal. Therefore, research is needed to investigate whether an array of seismic sources and receivers can be used to increase seismic energy levels

radiated into the seafloor and how the signal-to-noise ratio of the back-scattered seismic energy can be improved by beam forming and focusing the energy onto the UXO target. The current project addresses these questions based on numerical modeling, where seismic arrays are deployed in the water column and along the seafloor to radiate concentrated beams of energy into the seafloor sediments to improve the signal-to-noise ratio of seismic waves backscattered by UXO, and to improve the resolution of the location method.

This report summarizes the accomplishments of the SERDP seed project "Seismic Imaging of UXO-Contaminated Underwater Sites" over the first 4.5 months of the project including Tasks 1-3. The current research is intended as a first stage of a more extended project to locate and discriminate UXO in littoral environments based on seismic imaging methods. While this seed project addresses the problem of improving UXO detection using array techniques numerically, future research, if funded, will be directed towards physical modeling of the detection and in particular the discrimination of UXO based on seismic scattering techniques.

Task 1: Determination of Modeling Parameters at Mare Island, CA

The first task was concerned with the determination of physical parameters typical of littoral areas where UXO contamination is expected. These parameters are needed to build numerical models as a basis for finite-difference (FD) modeling, which is one of the primary tasks of the current SEED project. The parameters were chosen to be representative for a typical clean-up site (BRAC site) as in the case of the formal naval shipyard at Mare Island, Vallejo, CA. This site contains on- and off shore UXO contamination and has undergone several clean-up cycles in the past (mainly on shore). The physical parameters included seismic velocities and attenuation, mud densities and porosities, and sedimentary thickness to bedrock. In addition, the field parameters were complemented by estimates taken from the literature (Hamilton, 1971, 1972, 1976; Stoll, 1985; Kibblewhite, 1989) that are typical for these types of bay mud (clayey silts, and silty clays). The physical parameters were determined as:

<u>Salt Water Parameters</u>

P-wave velocity:	1510 m/s
S-wave velocity:	0 m/s
Density :	$1.03 \cdot 10^3$ kg/cm^3
Water depth:	1-3 m

<u>Bay Mud Parameters</u>

P-wave velocity:	1520 m/s – 1600 m/s (0-5 m depth)
S-wave velocity:	100 m/s – 150 m/s (0-5 m depth)
Wet Bulk Density:	$1.4 \cdot 10^3$ kg/cm^3
Porosity :	70 %
Sedimentary thickness:	> 10 m
Attenuation α:	0.2 dB/kHz/m
Quality factor Q:	88

These physical parameters were subsequently taken to build numerical models for wave propagation simulations using FD and analytical modeling.

Task 2: Analysis of Single Source Receiver Pairs

The second task was concerned with numerical FD modeling of single source and receiver combinations to investigate the amount of energy reflected and transmitted at the water-seafloor interface and scattered by the UXO. This investigation was carried out using 2-D FD models based on the physical parameters determined in Task 1. A schematic of the model is shown in Figure 1. The dimensions of the model were 6 m by 6 m with a water and sediment depth of 3 m each. Because the depth to bedrock was greater than 10 m at the Mare Island test site, the sediment/bedrock interface was not modeled, as the associated reflected waves would fall far outside the time interval of interest for reflections off the UXO. The parameters of the FD model are summarized in Table 1.

Table1: Finite Difference Modeling Parameters

	Salt Water Parameters	Bay Mud Parameters	UXO Parameters	Numerical Parameters
P-wave velocity [m/s]	1510	1520-1600	6568	
S-wave velocity [m/s]	0	0	3149	
Density [kg/m^3]	$1.03 \cdot 10^3$	$1.4 \cdot 10^3$	$2.7 \cdot 10^3$	
Depth [m]	3.0	3.0		
Quality Factor	∞	88	∞	
Length [m]	3.0	3.0		
Dimensions (x,z) [m]			0.3 by 0.1	
Node Spacing [m]				0.01
Number of Nodes (x,z)				600 by 600
Sample Interval [s]				10^{-5}
Frequency of Source (Ricker) Wavelet [Hz]				$5 \cdot 10^{+3}$

Various source signals and frequencies were investigated with the final signal being a Ricker wavelet (Gaussian derivative) with a central frequency of 5 kHz. The source frequency translates to a dominant wavelength of approximately λ_0=0.3 m for the P-wave in the bay sediments. Once the parameters were chosen, the FD code was tested for numerical stability to guarantee dispersion-free results. The single source-receiver experiment was intended to provide a baseline measurement for the reflection of seismic energy off the UXO and to evaluate the improvement using source-receiver arrays. A more detailed display of the velocity model, the locations of a single source, a receiver array, and a UXO are presented in Figure 2. The source and receiver array are located at a water depth of 1m, while the UXO is located 1 m below the water/sediment interface. While the velocity in water is homogenous at v_p=1510 m/s, the sediment-velocity is modeled by a tangential gradient from 1520-1600 m/s. The receiver array in Figure 2

consists of 31 receiver elements with a separation of 0.1 m. The seismic traces recorded from a shot located at x=1.0m and z=1.0 m are shown in Figure 3. Three arrivals are visible representing in sequence of arrival time the direct propagating P-wave, the P-wave reflected off the water/sediment interface, and the P-wave scattered of the UXO. It can be seen that the amplitudes of the UXO-scattered phases and the interface reflections are comparable in amplitude and separated in time for this shot geometry. Therefore, it should be possible to migrate the location of the UXO in space. However, for any given single source receiver pair, where the receiver is a pressure sensor, it is impossible to locate an object in space because of lack of directionality. In the present case, a migration of the signal recorded by the first receiver produced the results presented in Figure 4. In this case the migration was performed for a depth range between 2.5 m and 6.0 m only. Although the migrated amplitudes stack up along ellipses that touch the interface as well as the UXO, the exact location of the UXO or the interface cannot be determined. Similar to the seismic section in Figure 3, both signals reveal comparable amplitudes after migration. Therefore, the introduction of multiple receivers (pressure sensors) is necessary to determine the location of the UXO, which will also improve the signal to noise ratio.

Task 3: Analysis of Beam Forming Techniques for 1-D Source-Receiver Arrays

Source-Receiver Array Located in Water

The receiver array in Figure 2 consisted of 31 sensors, which can be used to steer a beam of recorded energy at any point in the medium. To illustrate this point the energy of a point pressure source located in a homogeneous medium at x=2.5 m and z=4.0 m is shown in Figure 5. It can be seen that the energy falls off gradually to all directions. If this energy is recorded with the receiver array located above the source, the array can be steered to illuminate the source location. The result of the beam forming is presented in Figure 6. It can be seen how the focused energy beam is centered on the source location and the width is greatly reduced compared to the energy radiated from the single source. In the same way, the array can be steered to illuminate each point of the medium to improve the detection of UXO in the subsurface.

The use of a full array of sources and receivers is presented in the next example where 31 sources are co-located with the receiver array from the previous example. In the present case a total of 961 seismograms were recorded, which contained reflections off the water/sediment interface and off the UXO as presented in Figure 3. The velocity model used for the migration was the same as for the FD modeling. The travel times from the source and receiver locations to each point in the subsurface were calculated using a 2-D eikonal solver (Podvin and Lecompte, 1991). The migration included the computation of the travel times for each source/receiver combination to each point in the medium below the array followed by stacking the root mean square (rms) amplitude over a predefined window on the seismogram. The resulting amplitude values are subsequently plotted as a function of location in the medium. The result of this migration is presented in Figure 7 for a depth range from 2.5 m to 6 m. A weak amplitude signature with values of 0.3 indicates the location of the water/sediment interface at 3 m depth.

Although the reflections from the interface and the UXO revealed comparable amplitudes in Figure 3, the averaging over the whole receiver array enhanced the phases scattered by the UXO, such that the migrated image shows a pronounced peak at the location of the UXO. The noise level of the migrated image is low, due to the high number of sources and receivers in the array. A cross section of the amplitude structure in Figure 7 is provided in Figure 8, where the amplitude is shown as a function of distance and depth across the model. It can be seen that the maximum of the amplitude coincides with the center of the UXO in x-direction, while it coincides with the top of the UXO in z-direction. The latter is caused by the impedance contrast between the top of the UXO and the sediment, which produces the reflected seismic signal. In addition to the UXO signature in z-direction, the water/sediment interface is indicated by an amplitude level of 0.3 at 3 m depth. The application of beam forming produced a sharp seismic signature of the UXO and a high signal to noise ratio evident by the low background amplitude level, which quickly decreases away from the UXO location.

In a natural environment there are numerous correlated and uncorrelated noise sources that have an adverse affect on the power and resolution of any detection algorithm. In the following example, the case of uncorrelated noise was examined, while correlated noise sources were treated in a later section. To test the stability of the inversion algorithm in the presence of noise, varying degrees of uncorrelated Gaussian distributed noise were added to the seismic waveforms shown in Figure 3 above. A waveform example with a noise level of 50% is presented in Figure 9. To compute a noise level that is related to the seismic UXO signal rather than the water/sediment interface reflections, the rms value of the seismic signal scattered by the UXO is computed as a basis for the noise. Therefore, the absolute noise level of each trace is distinct, based on the strength of the amplitudes scattered by the UXO as evident in Figure 9. The 50% noise level is high enough to obscure most of the scattered UXO signal between 4.0 ms and 4.5 ms on the seismogram (compare to Figure 3). This extreme case was chosen to test the performance of the source-receiver array. The result of the migration is presented in Figure 10 and should be compared to the noise-free situation of Figure 7. Although the noise level of the background is somewhat elevated, it is evident that the location of the UXO is correctly determined and the outline of the amplitude structure is comparable to that in Figure 7. At the same time the water/sediment interface is correctly located with an amplitude level equivalent to the noise-free case. The cross sections through the image reveal the elevated noise background in Figure 11, which is about 4% of the amplitude maximums. At the same time it can be seen that the shape of the amplitude structure in both cross sections is comparable to the noise-free example in Figure 8. This example illuminates the power of source-receiver arrays to stack coherent signals constructively while suppressing uncorrelated noise at the same time. This result is promising for UXO location in littoral environments that exhibit a lot of uncorrelated noise.

Source-Receiver Array Located on Seafloor

In order to obtain higher resolution images of the UXO the array of sources and receivers was located on the seafloor. In this case, the receivers consist of three-component motion- rather than pressure sensors, which simplifies the discrimination

effort of the UXO. However, in the current study, where the emphasis was on detection rather than discrimination, we concentrated on the vertical component of the recorded wavefield. A seafloor array with dimensions identical to those used in the last section is shown in Figure 12, where the location of the UXO is kept the same. The wavefield excited by the source located at x=1.0 m and z=1.0 m is presented in Figure 13. Two arrivals can be distinguished, which are the direct P-wave and the waves scattered by the UXO. It can be seen that the scattered waves are composed of several arrivals, which include phases reflected off the top of the UXO, followed by phases that reverberate internally within the UXO, and finally waves that are multiple reflected between the UXO and the water/sediment interface. The migration of these wavefields produces a strong amplitude maximum presented in Figure 14. Compared to the previous results the maximum is comprised of two peaks located towards the top edges of the UXO, which act as point scatterers reflecting the most energy. This feature is better resolved in the cross sections of the amplitude structure presented in Figure 15. It can be seen that the two maximums develop near the edges of the UXO, denoted by the dashed lines in Figure 15a. The vertical cross section in Figure 15b indicates that the maximum of the amplitude coincides with the top of the UXO as seen in Figure 8 before.

Considering the improved resolution of the seafloor array capable of detecting the edges of UXO under the current conditions, it is of interest to evaluate the case of two UXO in close proximity and to investigate possible interference effects. Such a situation is presented in Figure 16, where an additional (green colored) UXO with the same dimensions but different orientation is located at a distance of 0.1 m from the first. The resulting scattered phases show a more complicated pattern and some interference is visible on traces 15 to 20 in Figure 17. The interference is also evident in the migrated amplitude image shown in Figure 18. Two partially merged amplitude structures are visible above the UXO, with the vertically oriented UXO producing the weaker response, while the background noise is slightly elevated over the single UXO case (compare to Figure 14). To evaluate the amplitude maximums more closely, three cross sections were computed for this case. The cross section in x-direction is shown in Figure 19a, while two cross sections traversing each UXO in z-direction are presented in Figures 19b,c. The color-coding of the dashed lines is intended to better cross-reference the UXO between figures. The amplitude cross section exemplifies the interference between the seismic signals. While the amplitudes scattered by the (black colored) UXO on the left side are generally stronger than those scattered by the (green colored) UXO on the right side, the close proximity between them caused the scattered phases to interfere, producing reduced amplitude peaks for both UXO along the edge facing each other. Considering that the dominant wavelength of the incident wave is $\lambda_0 = 0.3$ m, this case might approach the limit of resolution in separating two closely positioned UXO. The cross sections in z-direction support earlier findings. The maximum amplitude related to the horizontally oriented (black colored) UXO in Figure 19b coincides with the top of the UXO as expected. However, interference between the two UXO caused the amplitude peak related to the vertically oriented (green colored) UXO to appear just below its top (Figure 19c).

Rippled Seafloor and Free Surface Effects

In most cases the seafloor is not flat as modeled in the previous examples but consists of a sinusoidal profile caused by continuous wave action. However, it may be difficult to determine the sinusoidal amplitude and wavelength in field applications and thus it is important to determine the effect of these parameters on imaging results. To address this question, finite difference computations were performed based on the model presented in Figure 20. This model is similar to the one used before except for a sinusoidal water/sediment interface with an amplitude of 0.04 m and a wavelength of 0.75 m (Lopes et al., 2003). Two models were computed, one with and the other without a free surface boundary condition for the water surface. A source gather of the model run without the free surface condition is presented in Figure 21. As previously the three phases are the direct wave, the interface reflection, and the waves scattered by the UXO. An interesting observation about the interface reflections is the focusing and de-focusing effect visible throughout the traces. This is caused by the sinusoidal nature of the interface that focuses the reflected amplitudes into the array from some troughs on the interface while it de-focuses the amplitudes from others. If the free surface boundary condition is included in the modeling, the recorded waveforms take on the form presented in Figure 22. It is evident that the reflection off the water surface has become the dominant arrival in the seismogram section. The effects of these wave phenomena on the migrated image will be shown in the next section.

The migration of the seismic waveforms is based on a velocity model with a flat water/sediment interface, because it is assumed that the amplitude and the wavelength of the sinusoidal interface are not known a priori. If the migrated area includes the region in the vicinity below the seismic array a mirror image of the water surface appears as the largest feature on the amplitude map at 2 m depth in Figure 23. This large anomaly suppresses the signature of the interface and the UXO as indicated in Figure 24, which shows the cross sections in x- and z-direction. It can be seen that the water surface signature is about twice as strong as that of the UXO. However, the geometry of the experiment prevented that multiples of the free surface reflection were recorded on the seismograms in Figure 22, such that the phases scattered by the UXO were recorded without interference. In this case the desired waveforms can be either separated in time on the seismograms, or the region where the free surface reflection appeared can be omitted during the migration procedure. In this case the phases stack destructively and will not be detectable elsewhere in the migration image. The result is shown in Figure 25, where the migration was limited to a depth greater than 2.5 m depth. It can be seen that the strongest amplitudes are now associated with the UXO signature. Because factors like water depth, speed of sound in water, and the expected depth range of UXO in sediments can be estimated well enough prior to most experiment, the source-receiver array can be positioned such that interference of water surface reflection multiples with UXO reflections will be minimized.

Although the migration was based on a velocity model with a flat seafloor, the result shows a correctly located interface that follows the sinusoidal character of the original boundary. The reason for this is the location of the source-receiver array straight above the interface. The near vertical raypaths, associated with the propagating waves, are very similar for the case of a flat or sinusoidal interface, such that travel time

differences are negligible. The fact that the migration yields the correct amplitude and wavelength of the interface and the correct location of the UXO despite the a priori assumption of a flat bottom has important consequences for the characterization of the UXO. With the obtained information of the actual interface the velocity model can be refined and the discrimination of the UXO, which depends more on an accurate velocity model, becomes more reliable. However, the discrimination is not part of the current project. A closer look at the interface signature in Figure 25 reveals that it is discontinues towards the outer limits of the source-receiver array depending on whether the peaks and troughs reflect the signal back into the array or outside of its limits. The cross sections in Figure 26 show the improvement over the results in Figure 24, where the amplitudes associated with the UXO become the dominant features again.

Search for Correct Velocity Gradient

The previous investigations were based on the use of the same velocity model for FD modeling and migration, with the exception of the sinusoidal model in the last section. The intention was to determine how beam forming can improve the energy radiation into the subsurface and how it can increase the resolution of the location process. Using a source-receiver array the velocity in the water can be estimated as well as in the top sediments if the array is lowered to the seafloor. However, the velocity-depth profile of the sediments is generally not known, and therefore, it is of interest to determine whether the velocity of the sediments can be estimated during the migration process.

The velocity model used in this project was based on a tangential gradient, which was found as a good representation of the velocity increase in the shallow subsurface in many geophysical applications. The currently used velocity gradient is shown in Figure 27. For an object located in the shallow subsurface small deviations from the correct velocity function are not too detrimental during the migration if the image is averaged over many sources and receivers of a seismic array. Thus, to increase the sensitivity of the migration on the velocity model, a UXO was placed in the sediments 2.5 m below the seafloor to increase the propagation distance of the waves between the array and the UXO. The geometry of this case is given in Figure 28, where the inversion result of the migration using the correct velocity gradient can be seen. If the correct velocity model is used the scattered phases are stacked constructively and located correctly during migration. Any deviation from the correct velocity model will produce incorrect shifts of the waveforms resulting in destructive interference during stacking and a reduced and spread amplitude image in space. Therefore, the amplitude of the UXO signature was used as a measure to determine the correct velocity gradient during migration. A total of 26 different velocity gradients were tested ranging from 1420 m/s to 1740 m/s as shown in Figure 29, where the correct gradient is indicated in red. For each gradient a separate migration was performed and the maximum of the UXO signature determined. The result is shown in Figure 30, where the maximum of each UXO signature is plotted as a function of velocity. The velocities represent the mean values of each gradient, while the dashed line indicates the mean velocity corresponding to the correct velocity gradient. It can be seen that the amplitude maximum coincides with the correct velocity function as the migration produces the strongest amplitude image. However, it is also evident that the

maximum is broad and that comparable high amplitude values were obtained for a range of velocities. This indicates that the migration process will produce similar equally good results even if the correct velocity gradient is not known. It should be kept in mind that this investigation was carried out for a UXO located at a sediment depth of 2.5 m, while in the majority of cases UXO are expected to be located at shallower depths where the influence of the correct velocity gradient is even less pronounced. This result seems promising for the location of UXO in shallow marine environments using seismic source-receiver arrays.

Conclusions

Seismic arrays are very well suited for beam forming, particularly in homogeneous media where the velocities of the propagating waves are known, such as in water. While the success of UXO detection is comparable between an array located in the water column and an array located on the seafloor, the latter has much better resolution, because of the proximity to the UXO. Additionally, the applicability of 3-component motion sensors in a seafloor array will increase the resolution of the detection method - and eventually of the discrimination as well. Low signal-to-noise situations can be overcome by the use of source-receiver arrays, where the ability to stack can enhance seismic UXO signatures that otherwise remain undetected. There are currently worldwide efforts under way to develop monitoring techniques based on stacking approaches that are capable of detecting minute signals from remote sources in noisy environments. The application of array techniques to UXO detection follows the same principle. It is promising that the dimensions of two UXO, separated by one third of the wavelength of the incident wave, can be resolved if the targets are located within a few wavelengths of the array. The findings that the parameters of a rippled seafloor can be determined while UXO are correctly located in the sediments, even if a flat seafloor interface is assumed during the migration process, has far reaching consequences. The newly found interface parameters help to improve the velocity model, which increases the resolution of the applied method, and eventually will lead to better discrimination techniques that rely on seismic scattering. Furthermore, the result that a range of comparable velocity models yields similar location accuracy is also attributable to the use of a source-receiver array, which reduces small mislocation errors through stacking. However, these findings need to be further investigated with physical modeling.

Literature:

Hamilton, E. L., 1971, Prediction of in-situ acoustic and elastic properties of marine sediments, *Geophysics*, Vol. 36, No.2, p. 266-284.

Hamilton, E. L., 1972, Compressional-wave attenuation in marine sediments, *Geophysics*, Vol. 37, No.4, p. 620-646.

Hamilton, E. L., 1976, Prediction of in-situ acoustic and elastic properties of marine sediments, *Geophysics*, Vol. 41, No.5, p. 983-996.

Kibblewhite, A. C., 1989, Attenuation of sound in marine sediments: A review with emphasis on new low-frequency data, *J. Acoust. Soc. Am.*, Vol. 86, No.2, p. 716-738.

Lopes J. L., Nesbitt C. L., Lim R., Williams K. L., Thorsos E. I. and, Tang D., 2003, Subcritical Detection of Targets Buried Under a Rippled Interface: Calibrated Levels and Effects of Large Roughness, Proceedings Oceans 2003 Marine Technology and Ocean Science Conference, San Diego, CA.

Stoll, R. D., 1985, Marine Sediment Acoustics, *J. Acoust. Soc. Am.*, Vol. 77, p. 1789-1799.

Podvin, P. and Lecompte, I., 1991, Finite difference computations of travel times in very contrasted velocity models: A massively parallel approach and its associated tools, *Geophys. J. Int.*, Vol. 105, p. 271-284.

Figures

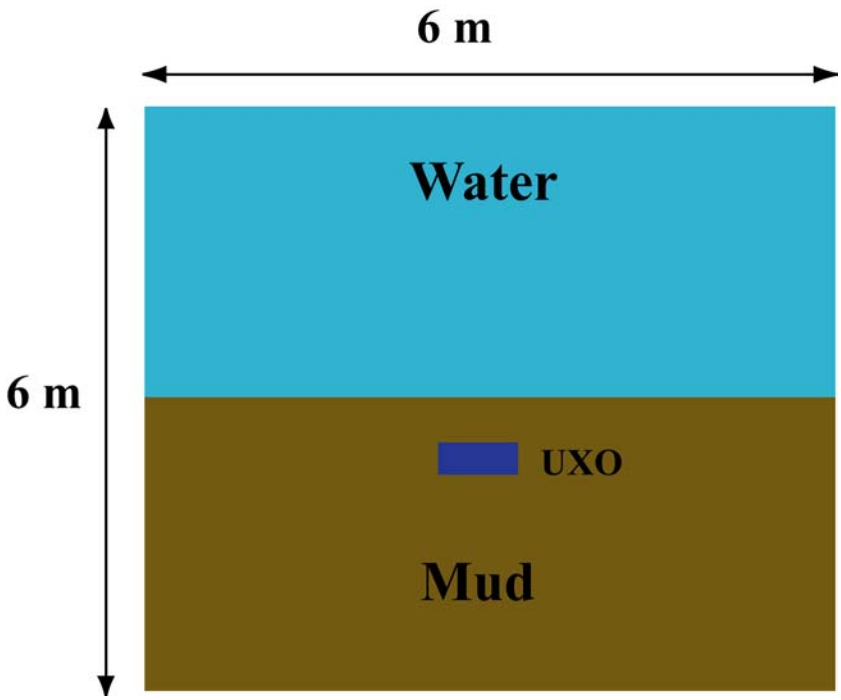

Figure 1: Schematic of the finite difference model

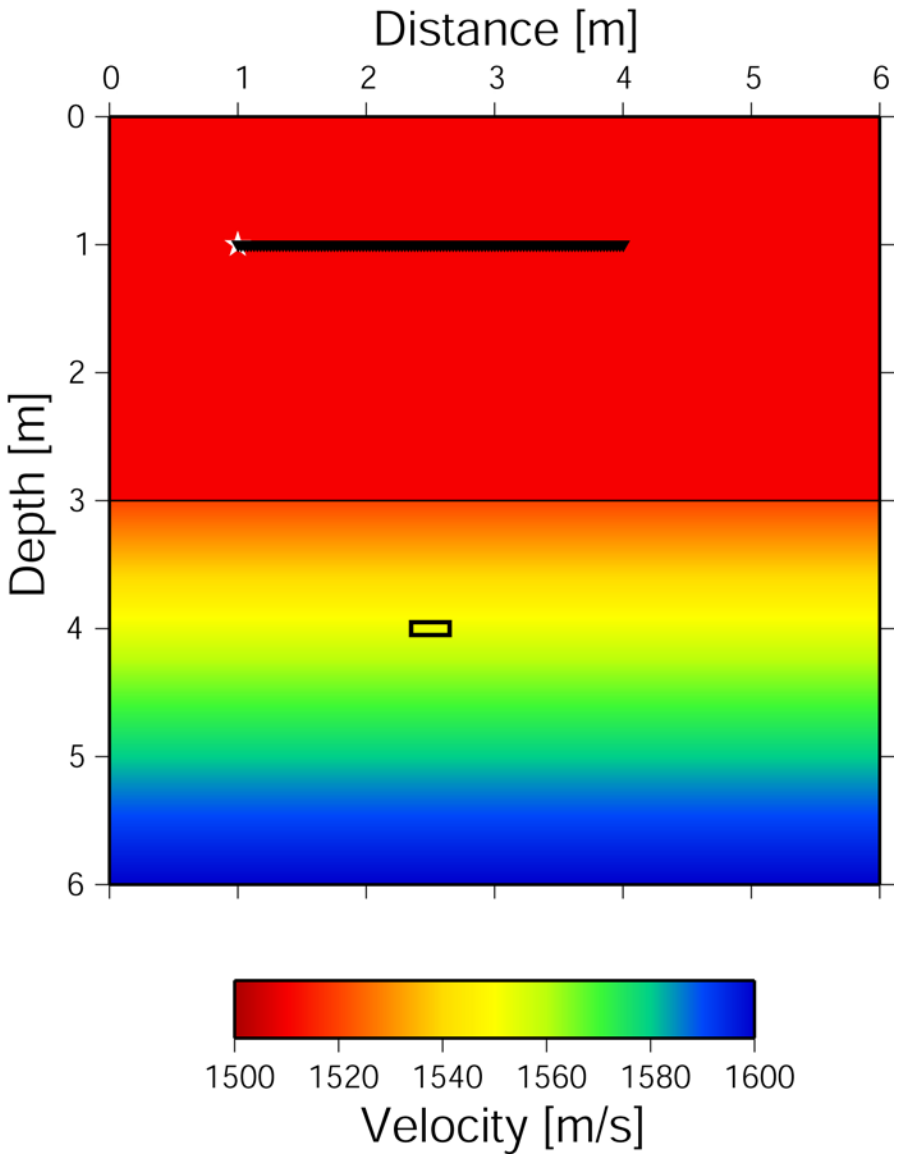

Figure 2: Velocity model derived from the parameters listed in Table 1. Source number one is indicated by the white star, while the receiver array, consisting of 31 sensors, is denoted by black triangles. The water layer is represented by the top 3 m, while the sediments are represented by the bottom half.

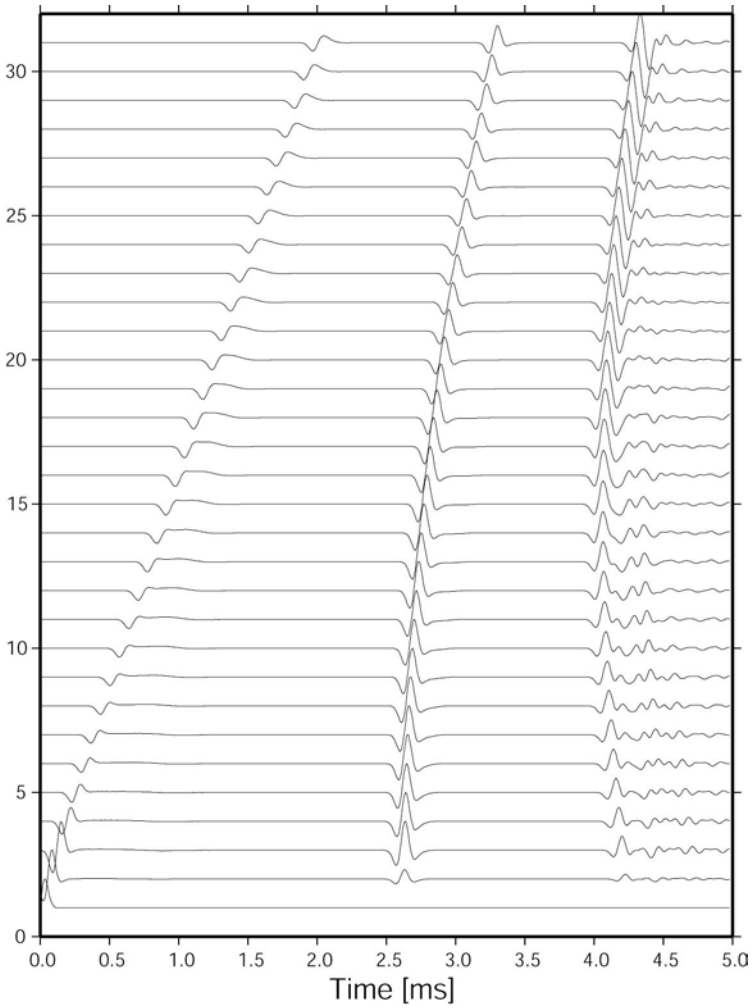

Figure 3: Seismic waveforms generated for the model shown in Figure 2. The source location was at x = 1 m and z = 1 m.

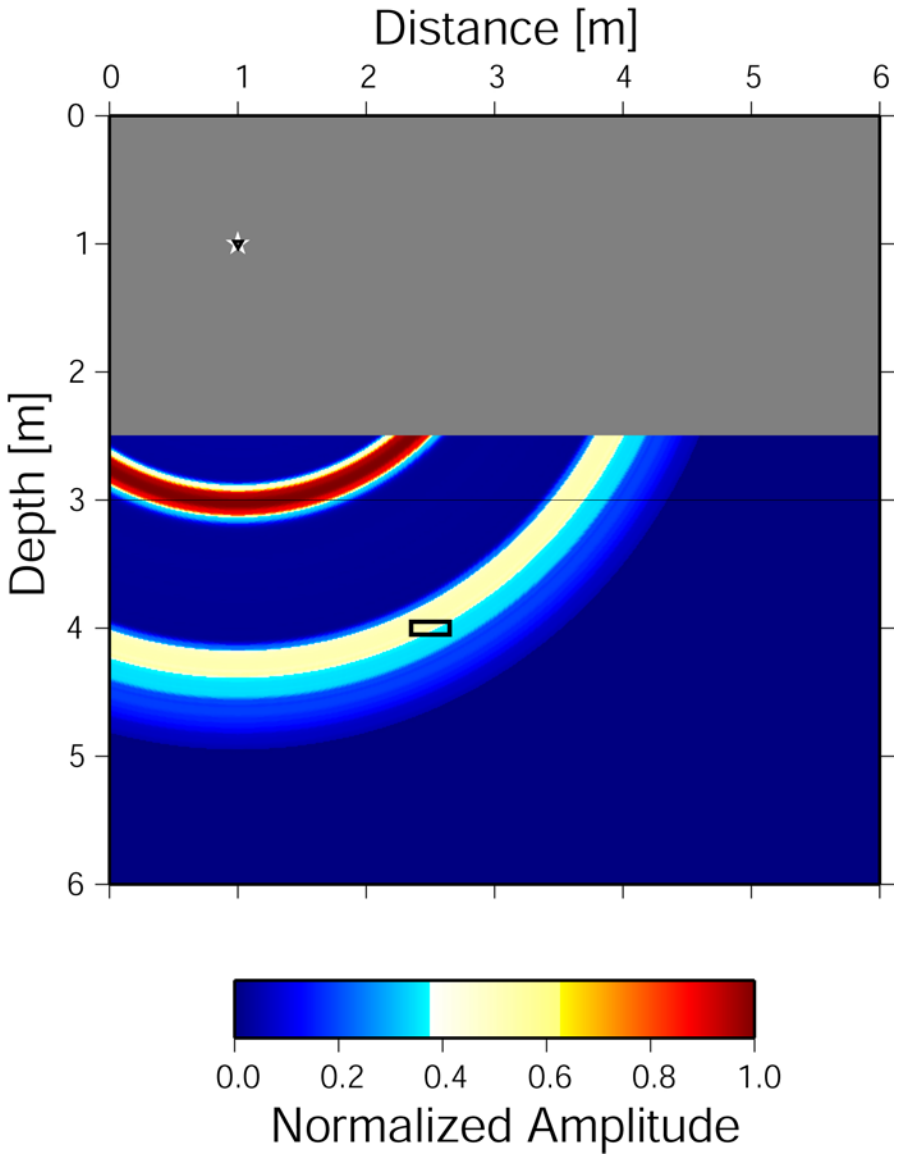

Figure 4: Migration result of a single source-receiver combination. The image is based on a source and receiver both located at x = 1 m and z = 1 m, indicated by the star and triangle, respectively.

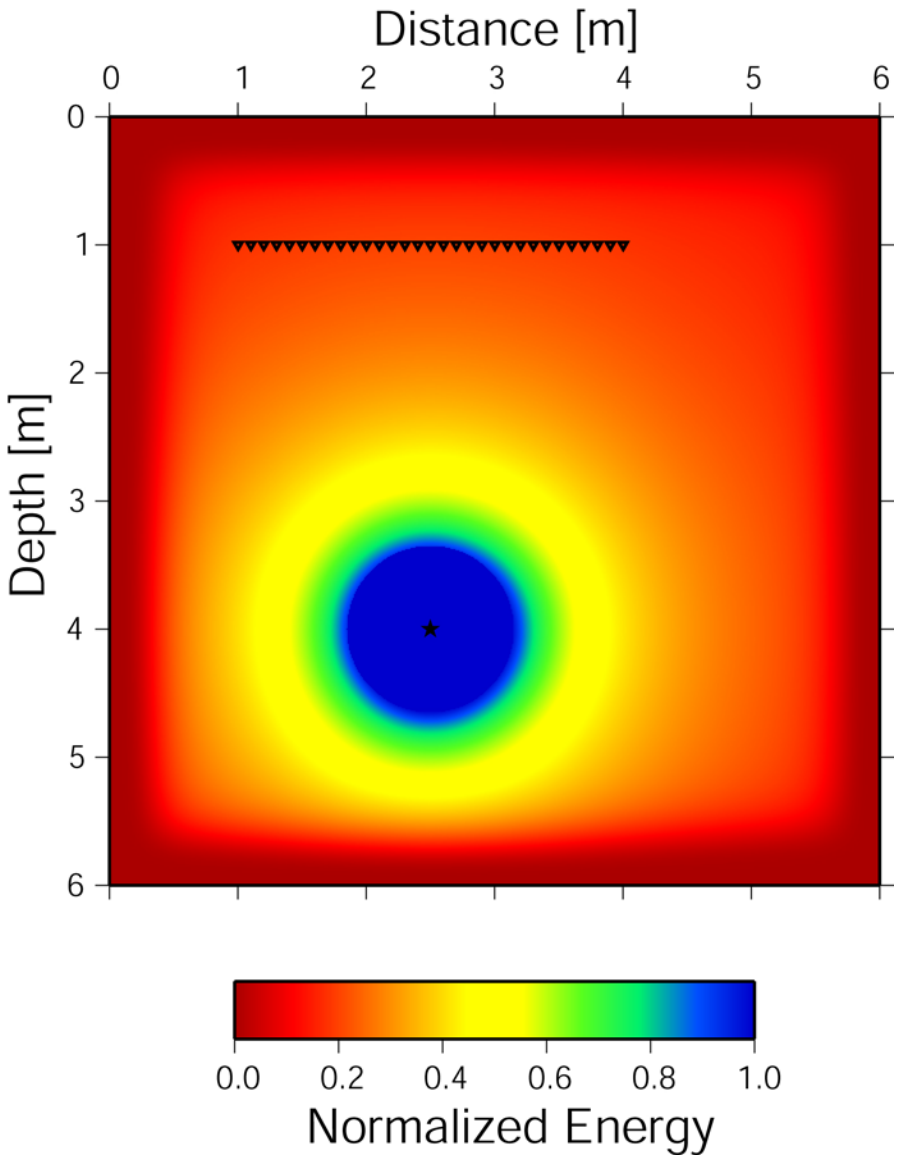

Figure 5: Energy radiation of a point pressure source located in a homogeneous medium. The gradual decay in radial direction is evident, while the energy in central source region was normalized for plotting purposes.

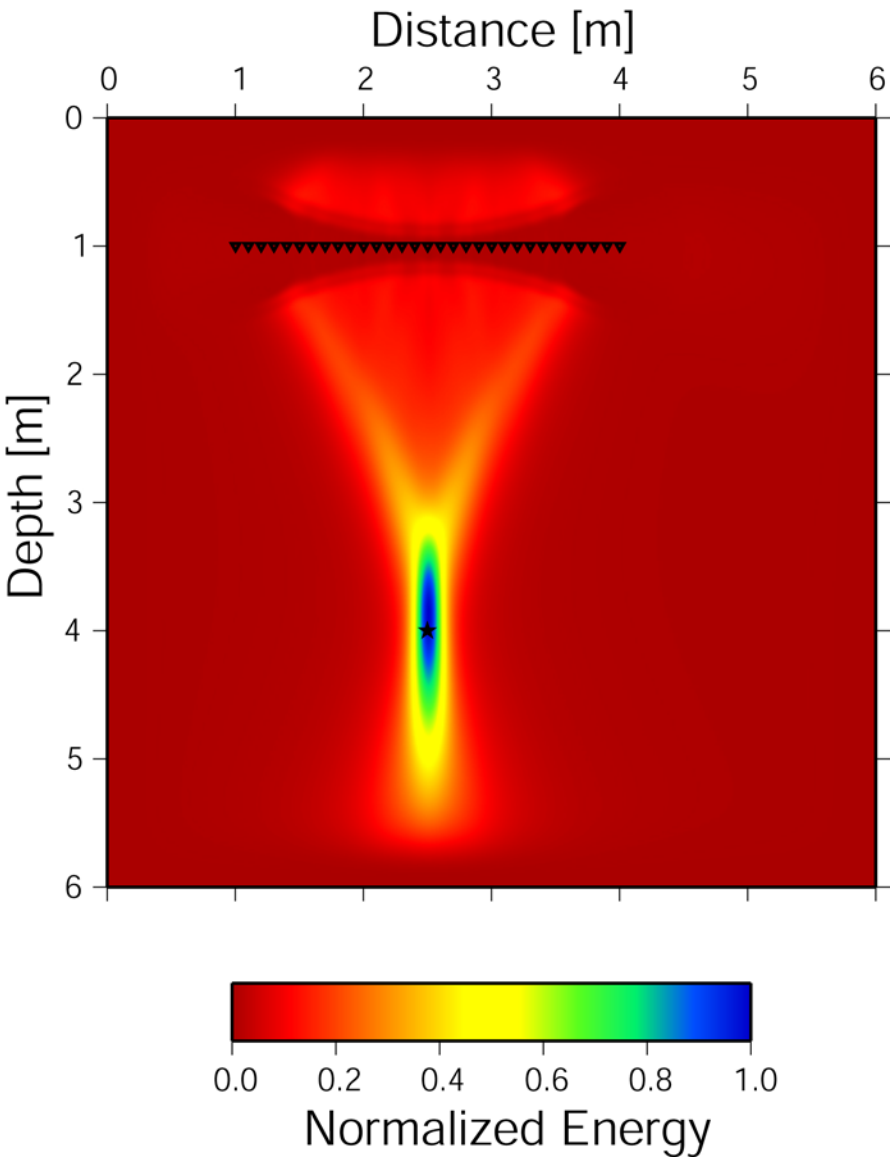

Figure 6: Result of beam forming obtained by steering the receiver array to illuminate the source location. The recorded energy was emitted by the source in Figure 5.

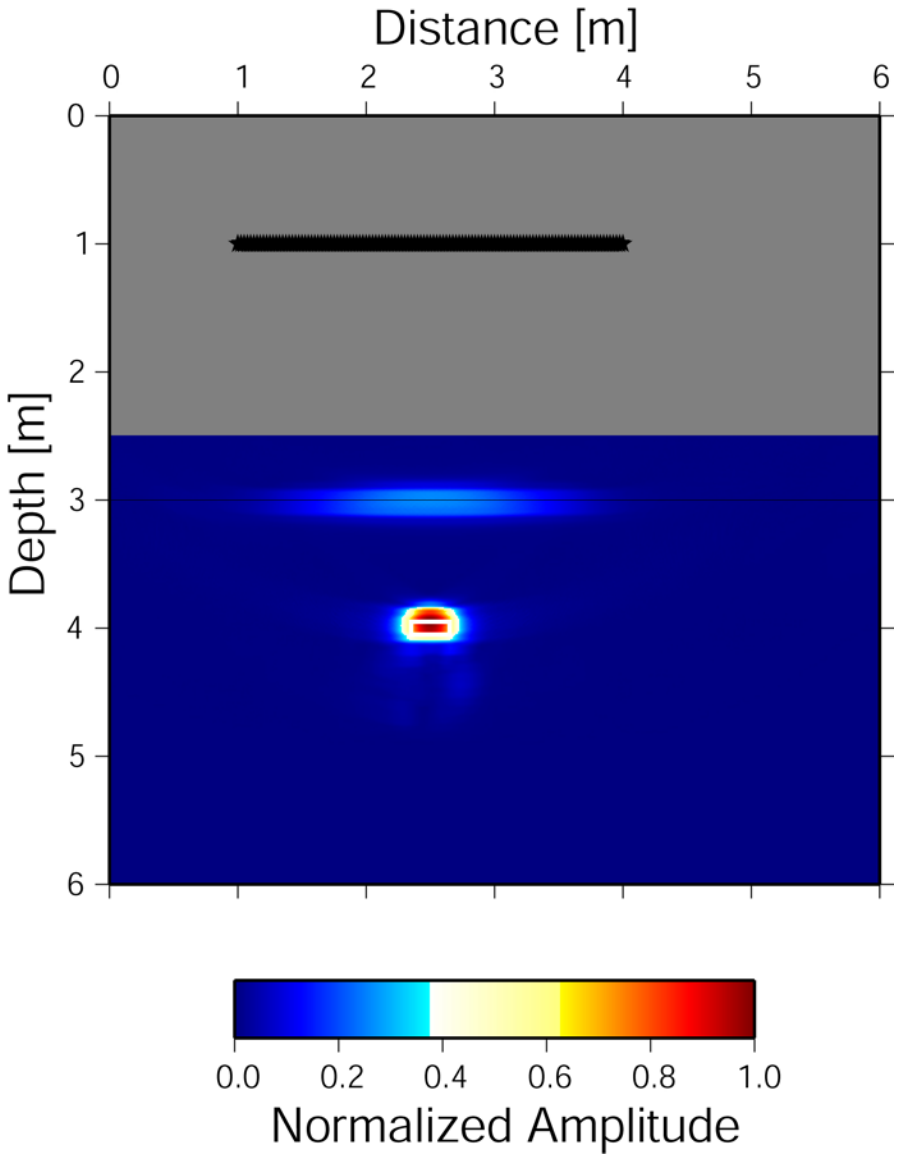

Figure 7: Normalized amplitude map of migrated waveforms recorded by 31 sources and 31 receivers in the source-receiver array, co-located at a depth of 1 m between x=1 m and x=4 m.

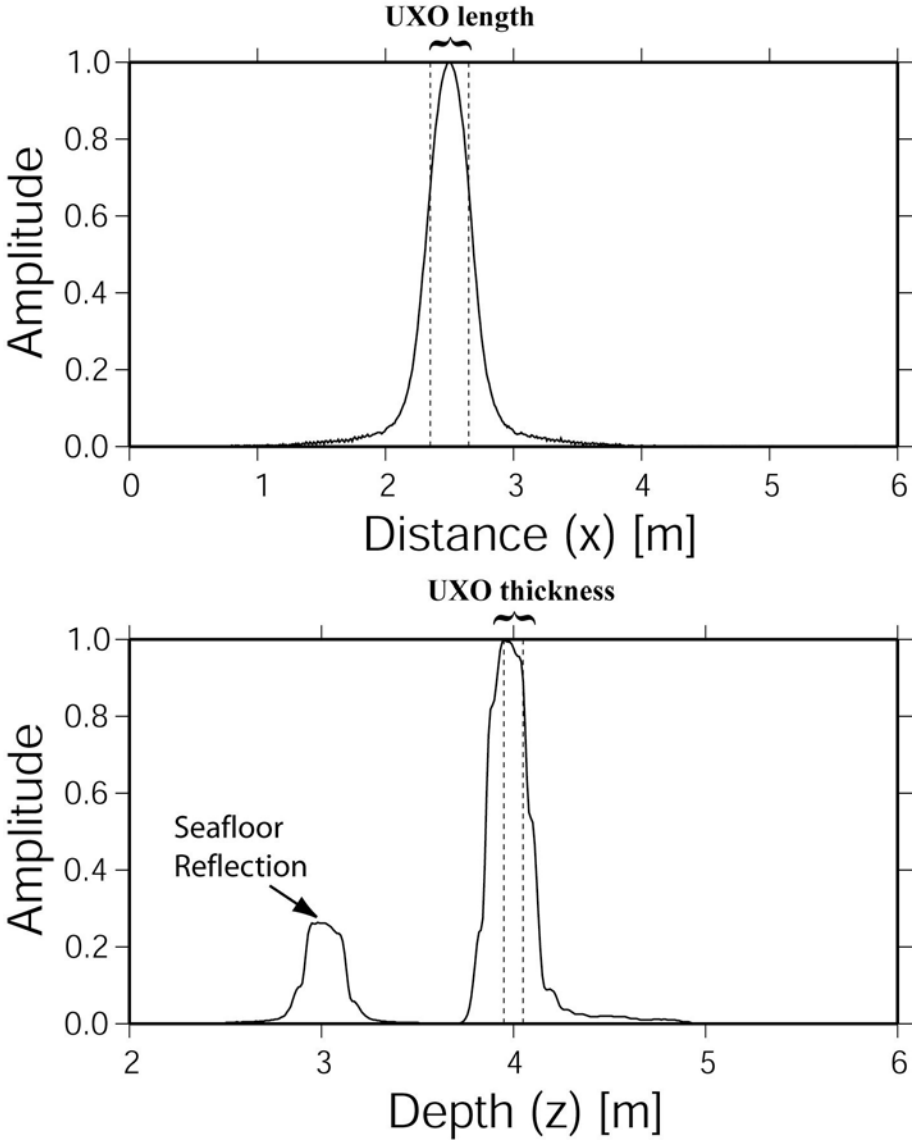

Figure 8: Cross sections of normalized amplitudes through the UXO signature in Figure 7. **a)** Cross section in X-direction.
b) Cross section in z-direction.

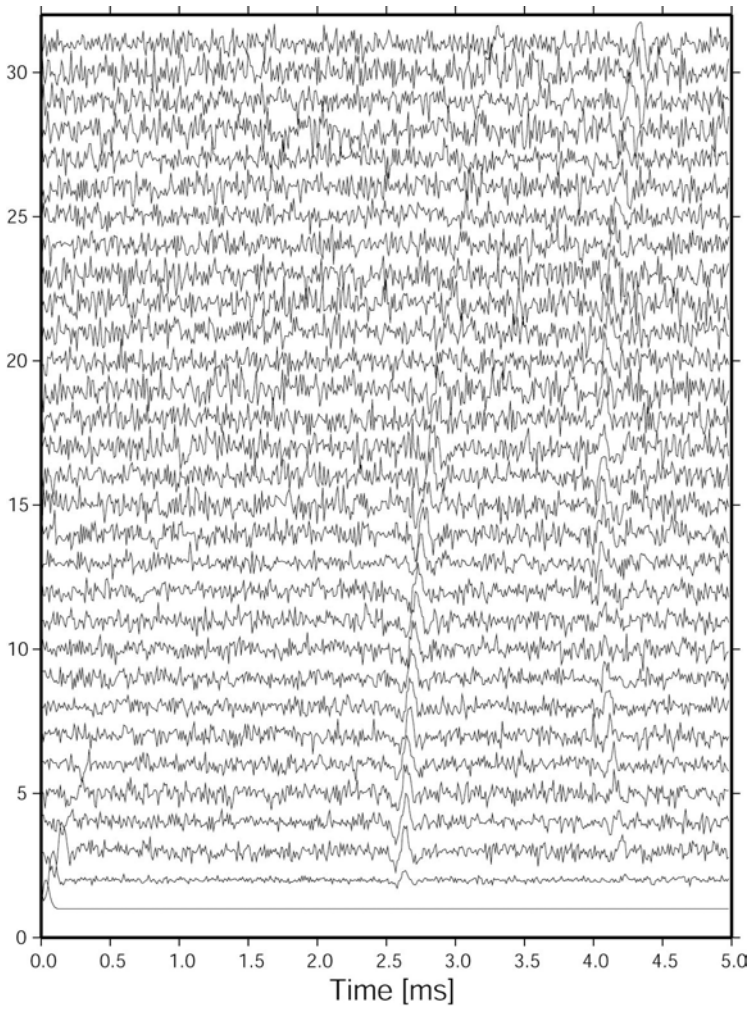

Figure 9: Same as Figure 2 with the addition of 50% Gaussian distributed noise.

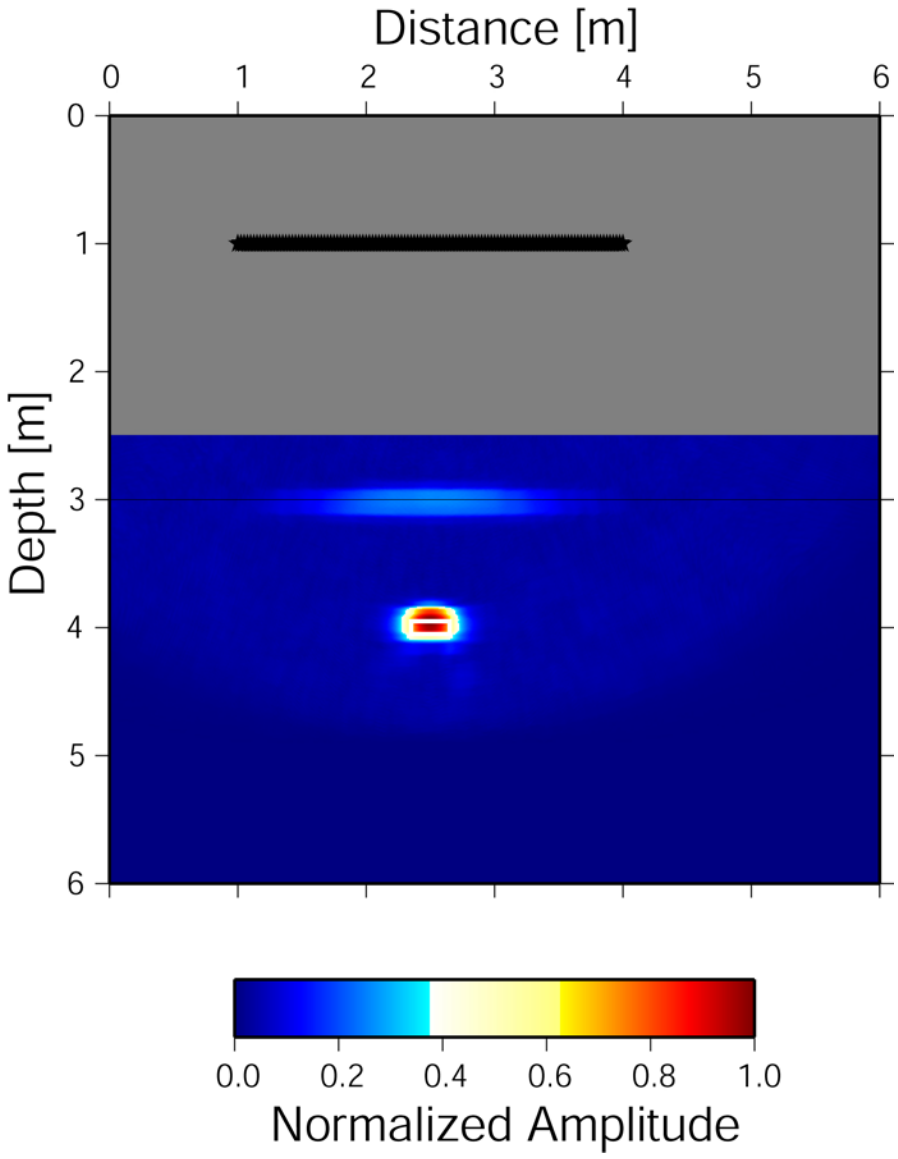

Figure 10: Normalized amplitude map of migrated waveforms recorded by 31 sources and 31 receivers in the source-receiver array. A noise level of 50% was added to the waveforms prior to migration.

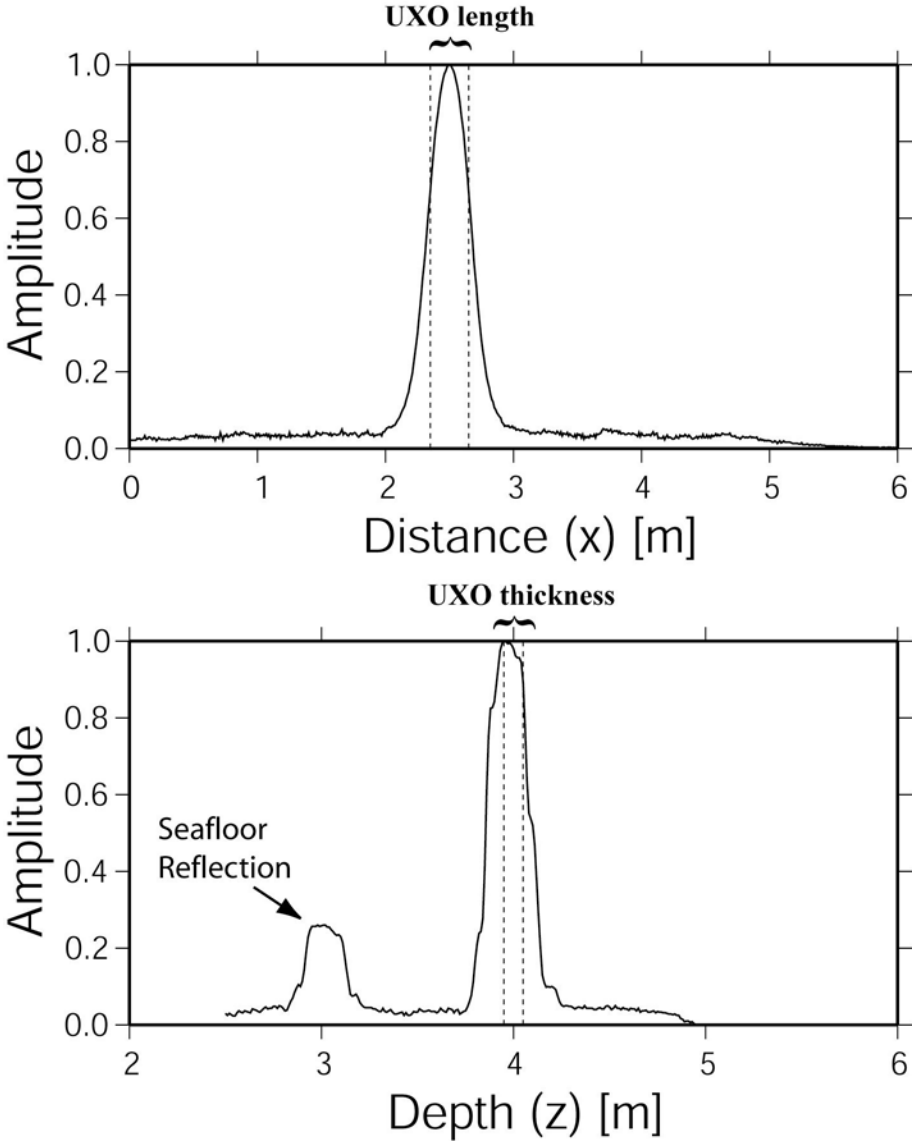

Figure 11: Cross sections of normalized amplitudes through the UXO signature in Figure 10. **a)** Cross section in X-direction. **b)** Cross section in z-direction.

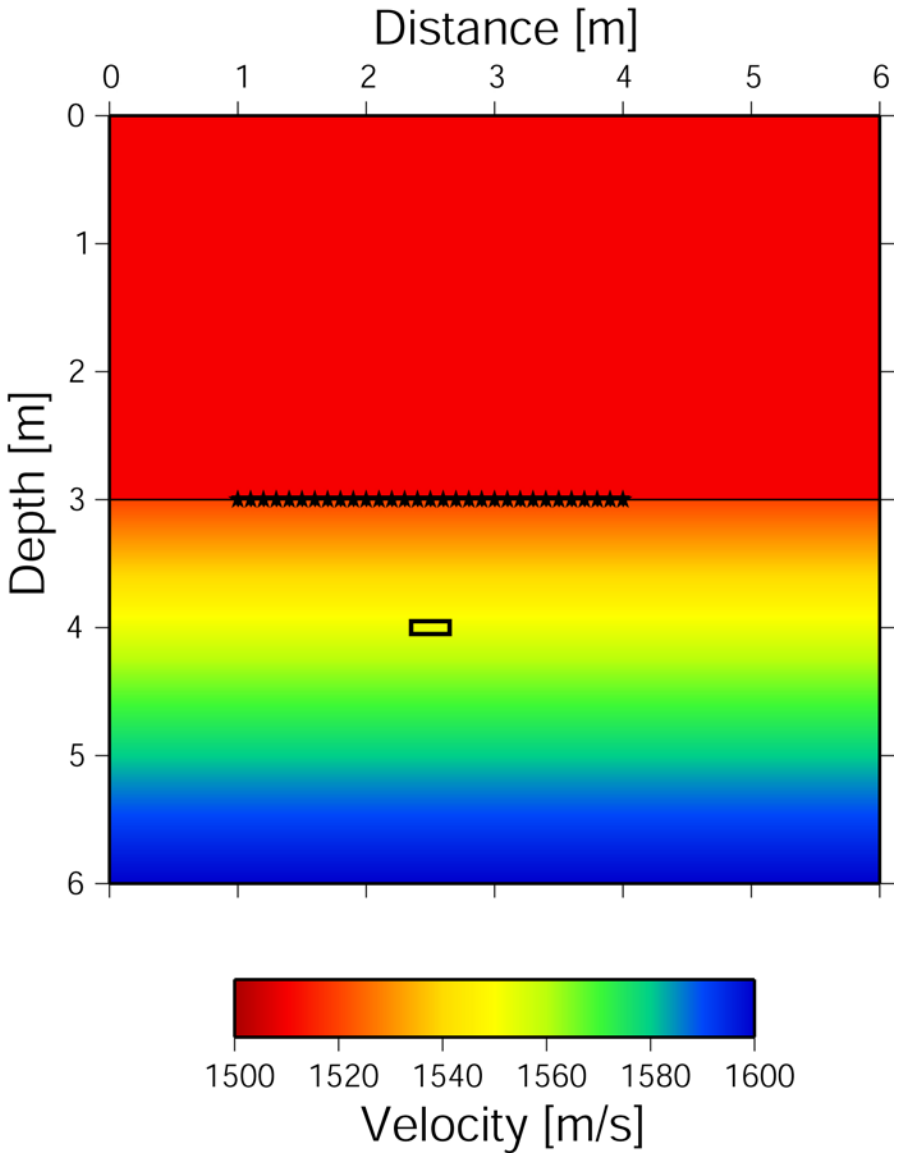

Figure 12: Same velocity model as in Figure 2 with source-receiver array positioned along seafloor.

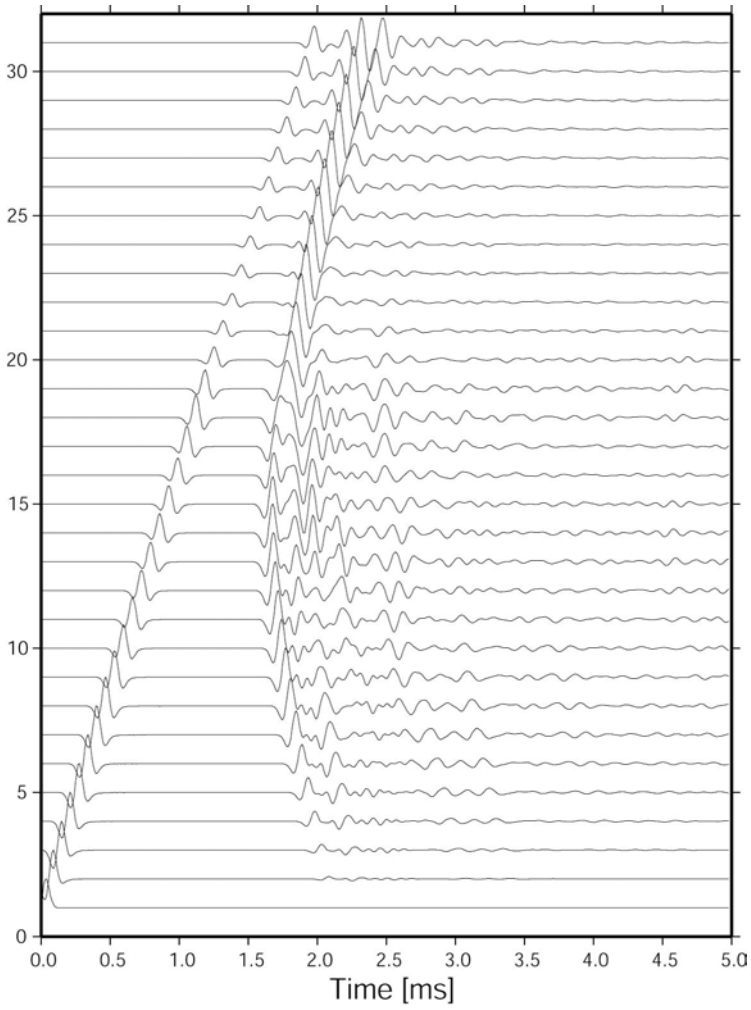

Figure 13: Seismic waveforms generated by the shot at x = 1m and z = 3 m and recorded by the receiver array with the model shown in Figure 12.

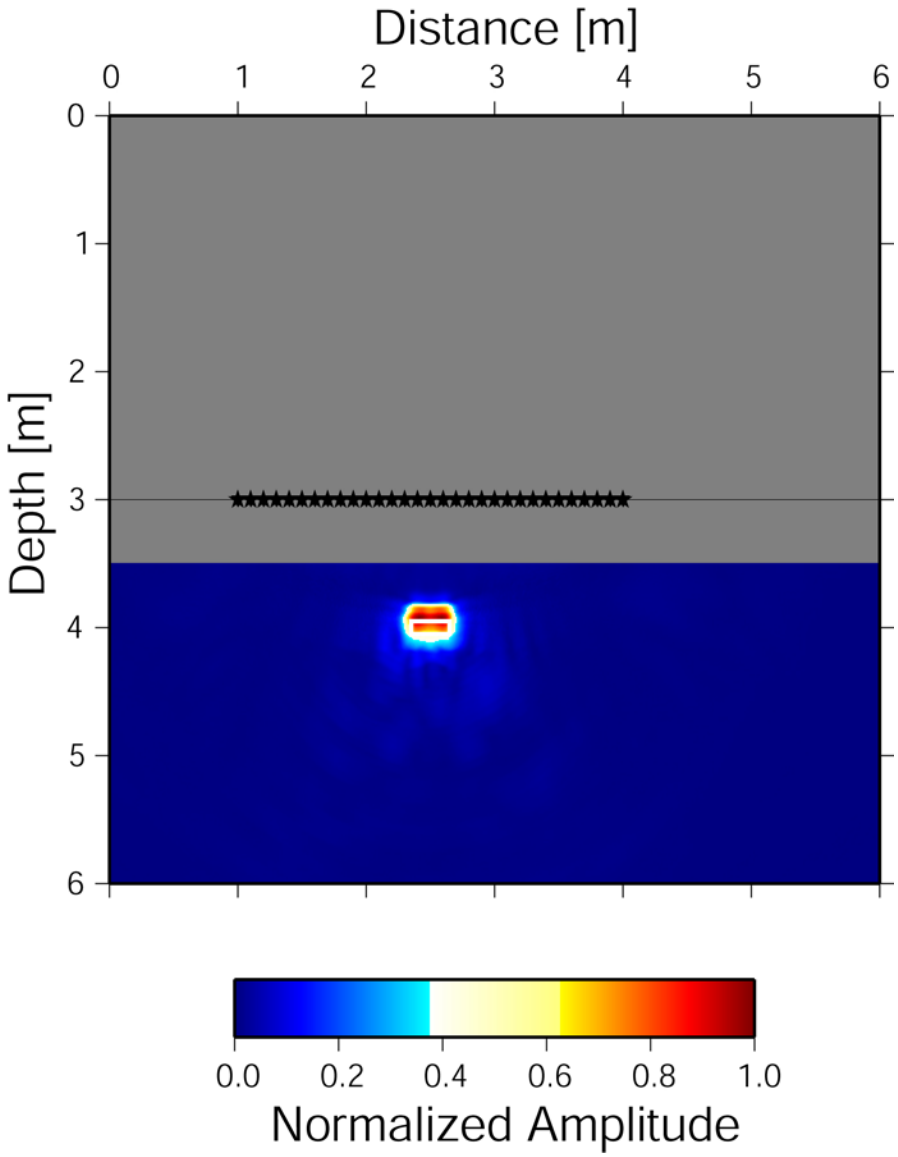

Figure 14: Normalized amplitude map of migrated waveforms recorded by the 31 sources and 31 receivers in the seafloor array.

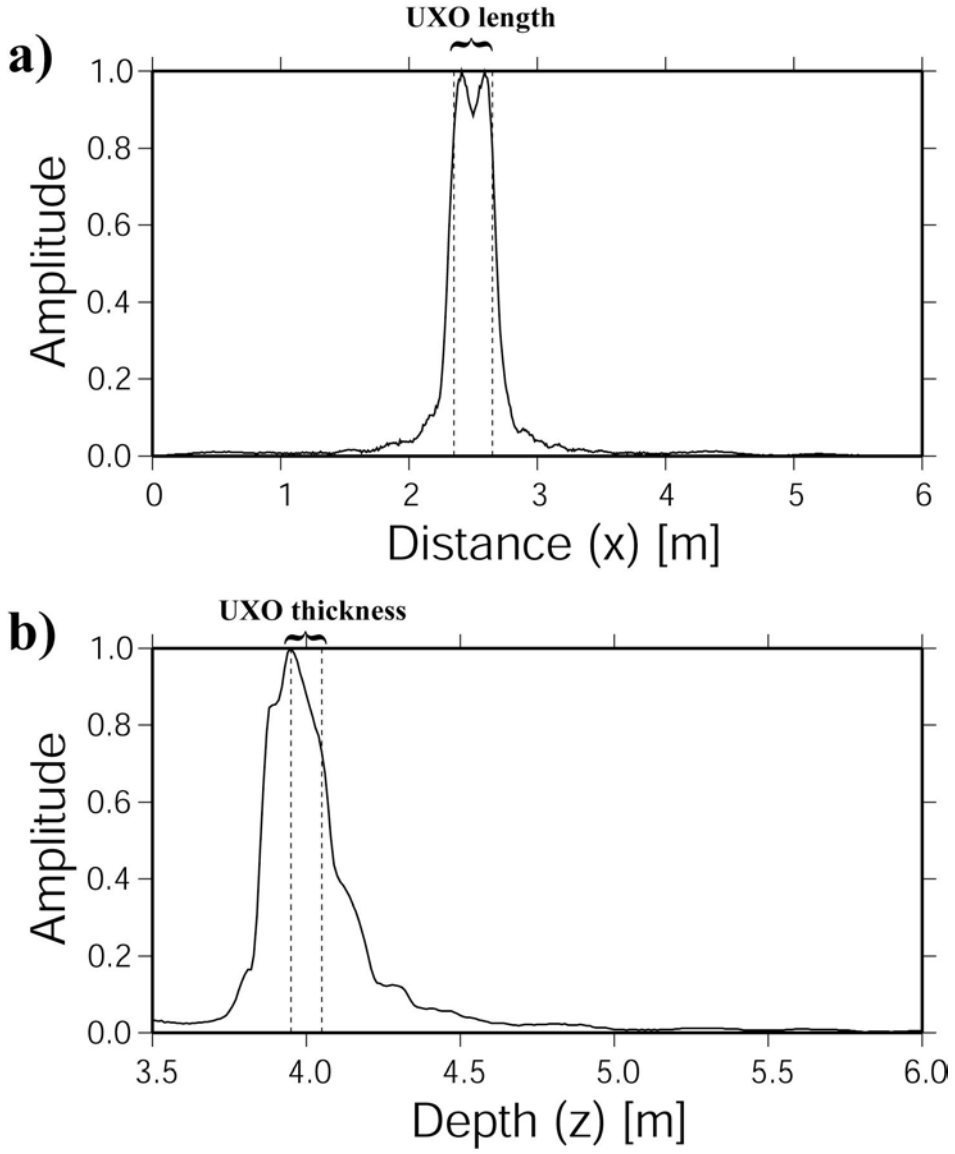

Figure 15: Cross sections of normalized amplitudes through the UXO signature in Figure 14. **a)** Cross section in X-direction.
b) Cross section in z-direction.

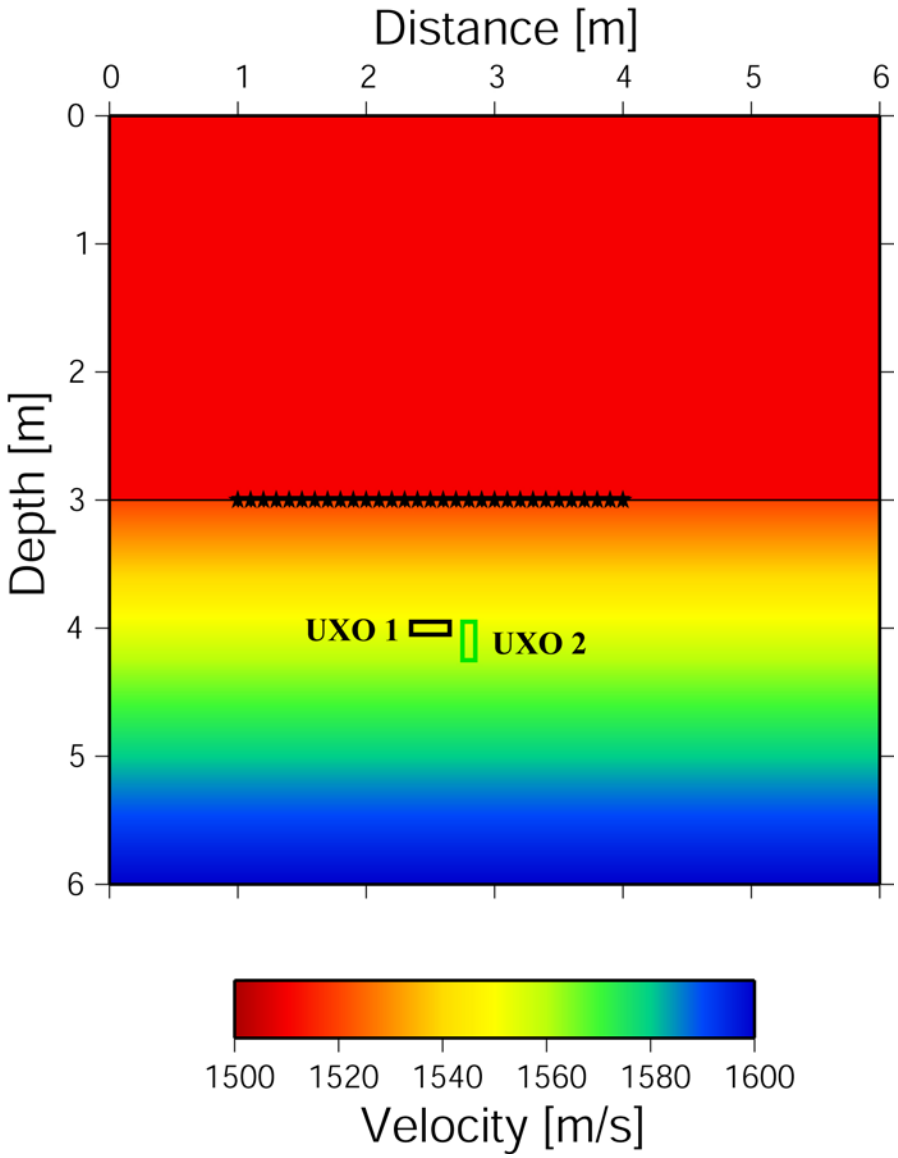

Figure 16: Same velocity model as in Figure 2 with source-receiver array positioned along seafloor. Two UXO are modeled and color-coded for better comparison with Figures 18 and 19.

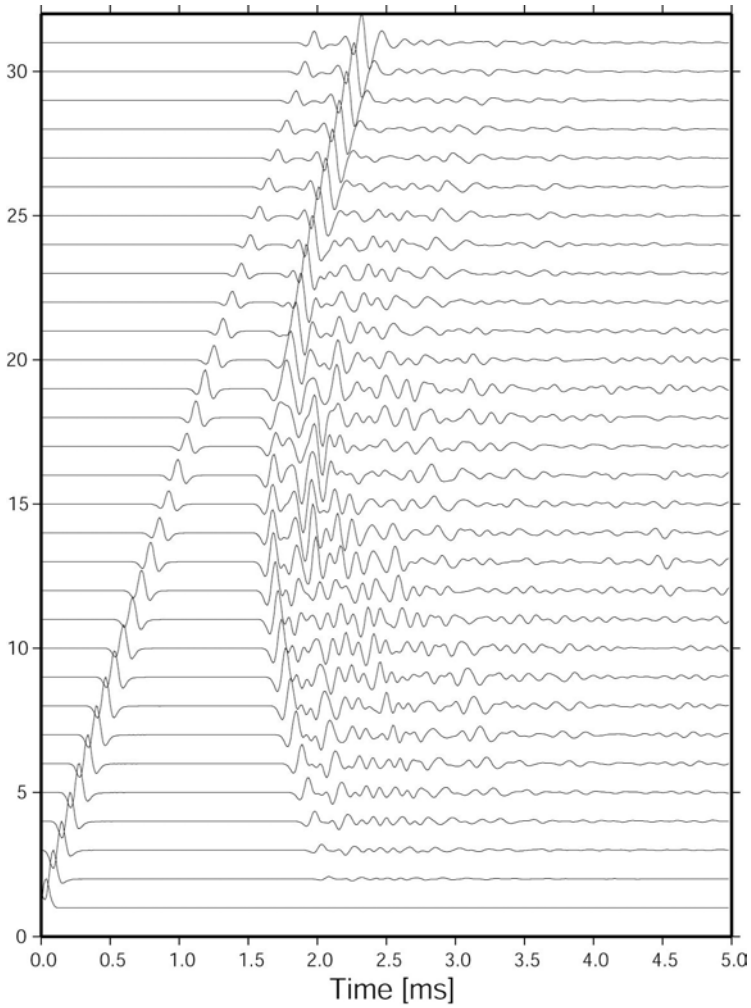

Figure 17: Seismic waveforms generated by the shot at x = 1m and z = 3 m and recorded by the receiver array with the model shown in Figure 16.

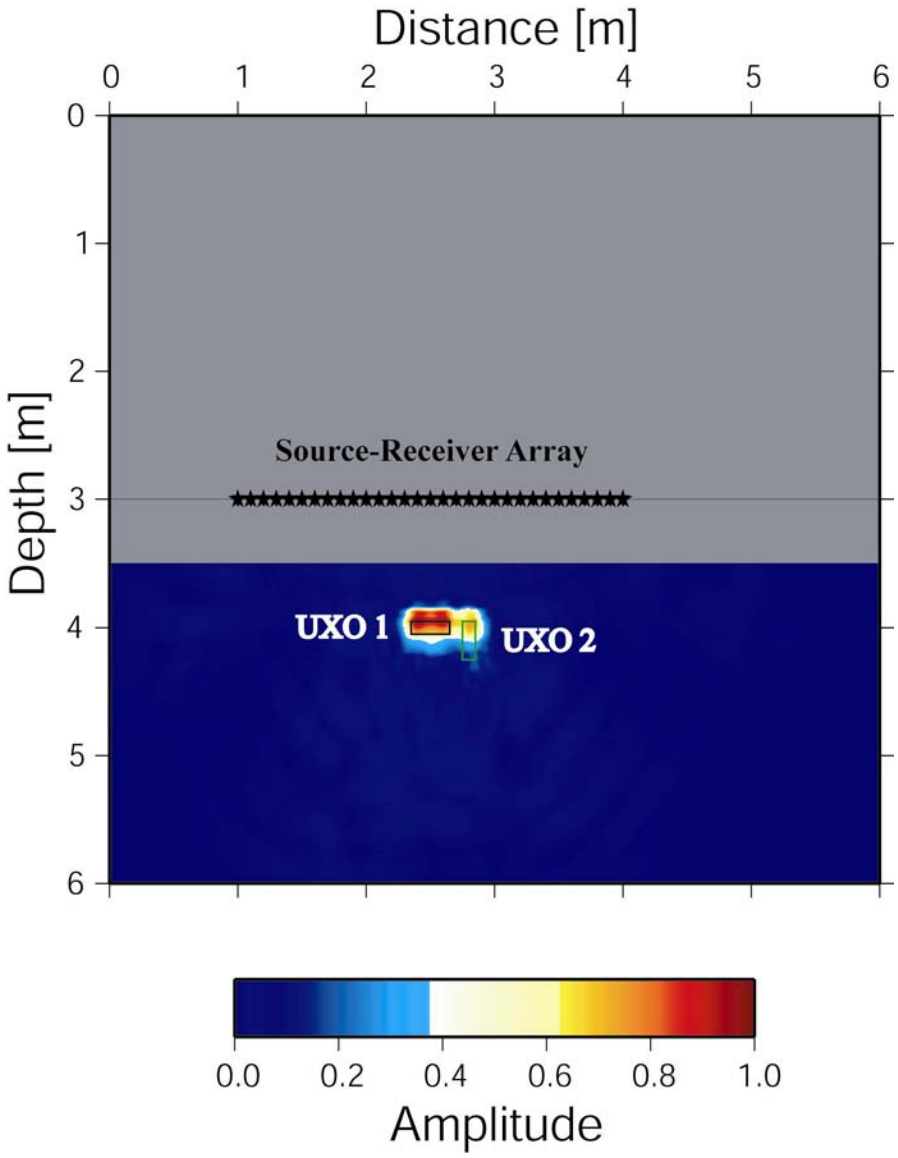

Figure 18: Normalized amplitude map of migrated waveforms recorded by the 31 sources and 31 receivers in the seafloor array.

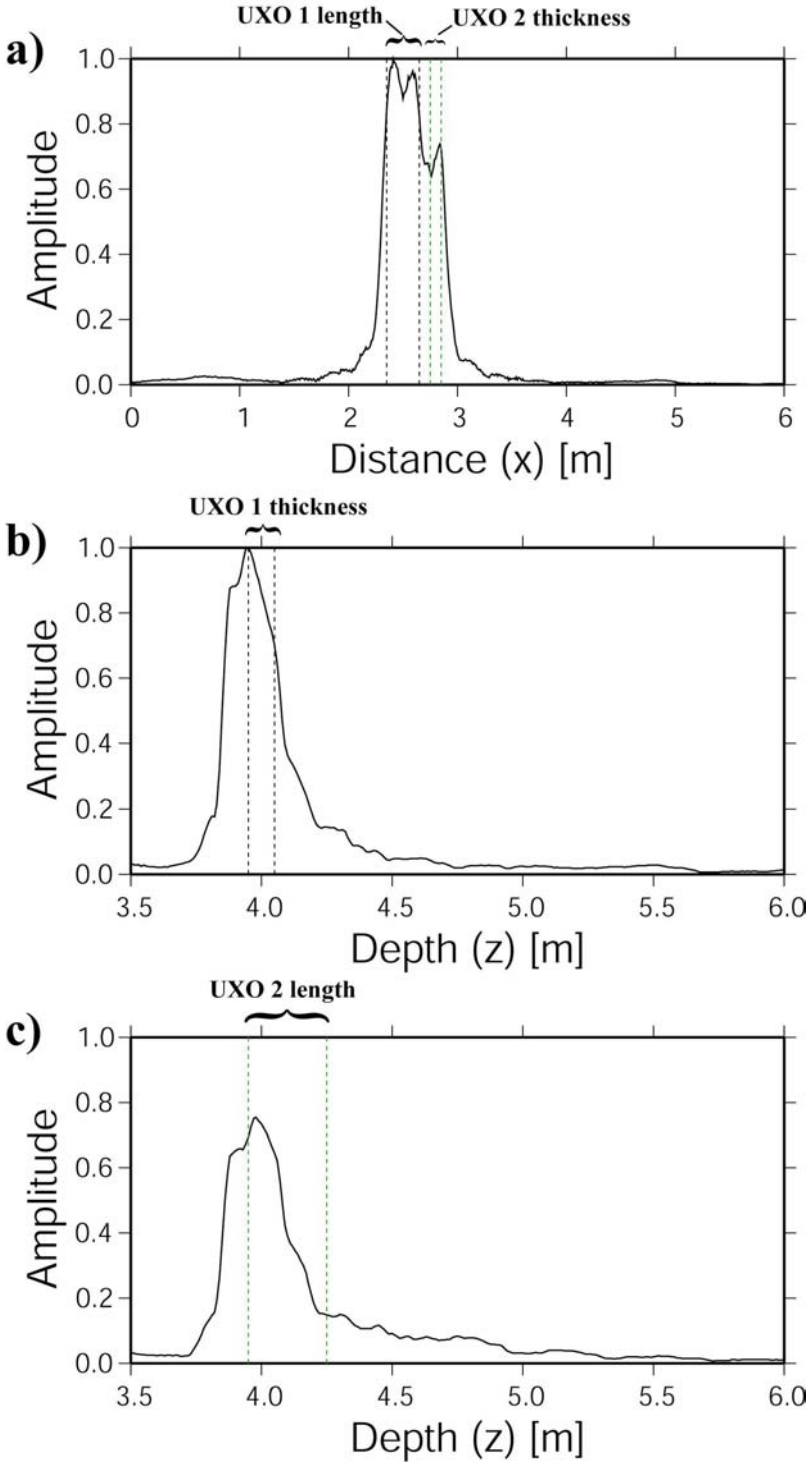

Figure 19: Cross sections of normalized amplitudes through the UXO signature in Figure 18. Colored dashed lines refer to colored UXO in Figures 16 and 18. **a)** Cross section in X-direction. **b)** Cross section in z-direction.

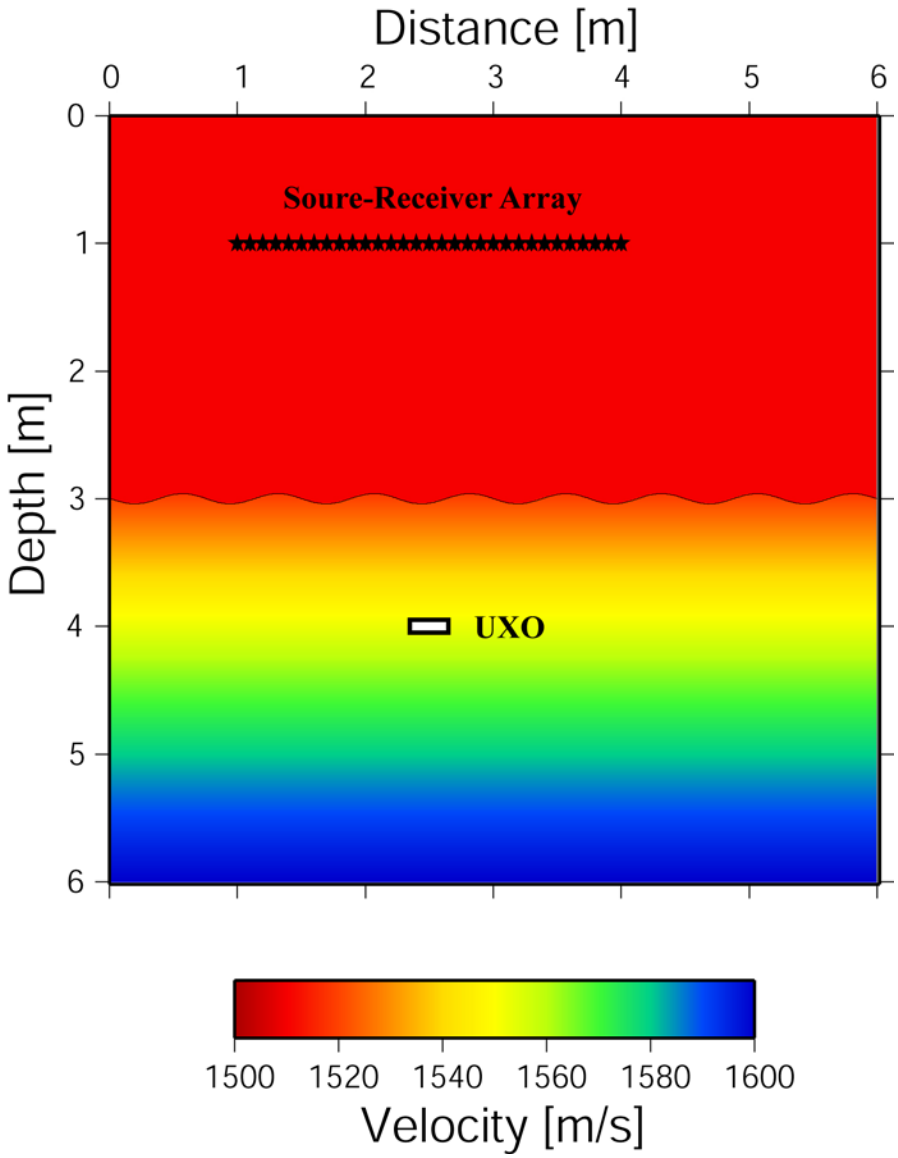

Figure 20: Same velocity model as in Figure 2 with the difference of a rippled seafloor.

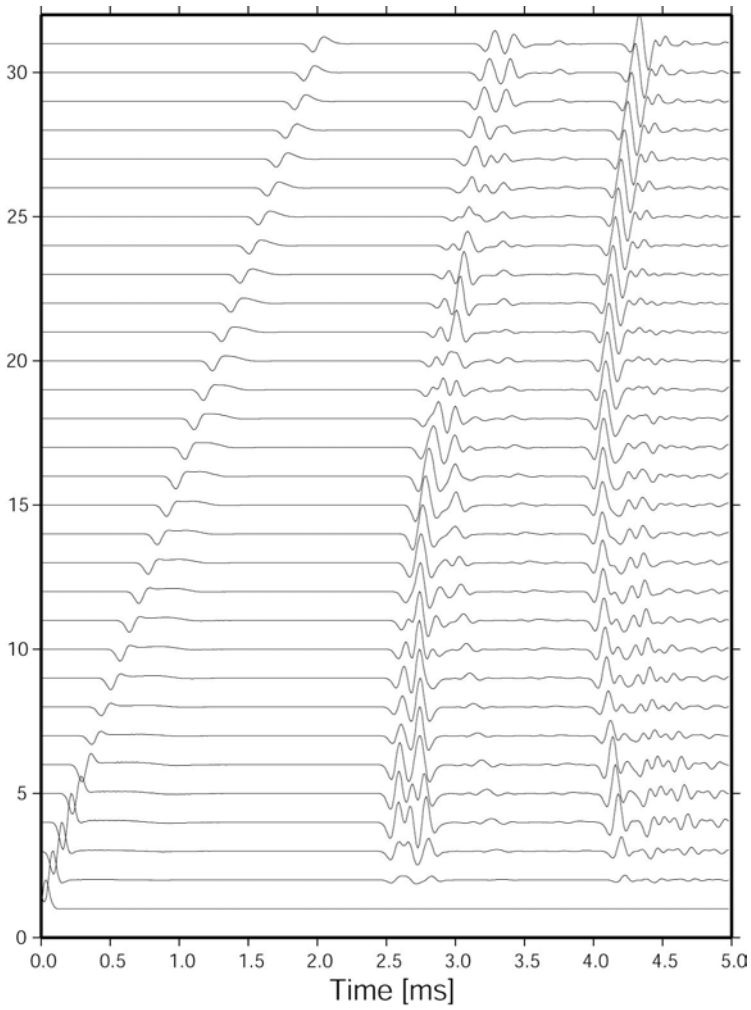

Figure 21: Seismic waveforms generated by the shot at x = 1m and z = 1 m and recorded by the receiver array with the model shown in Figure 20.

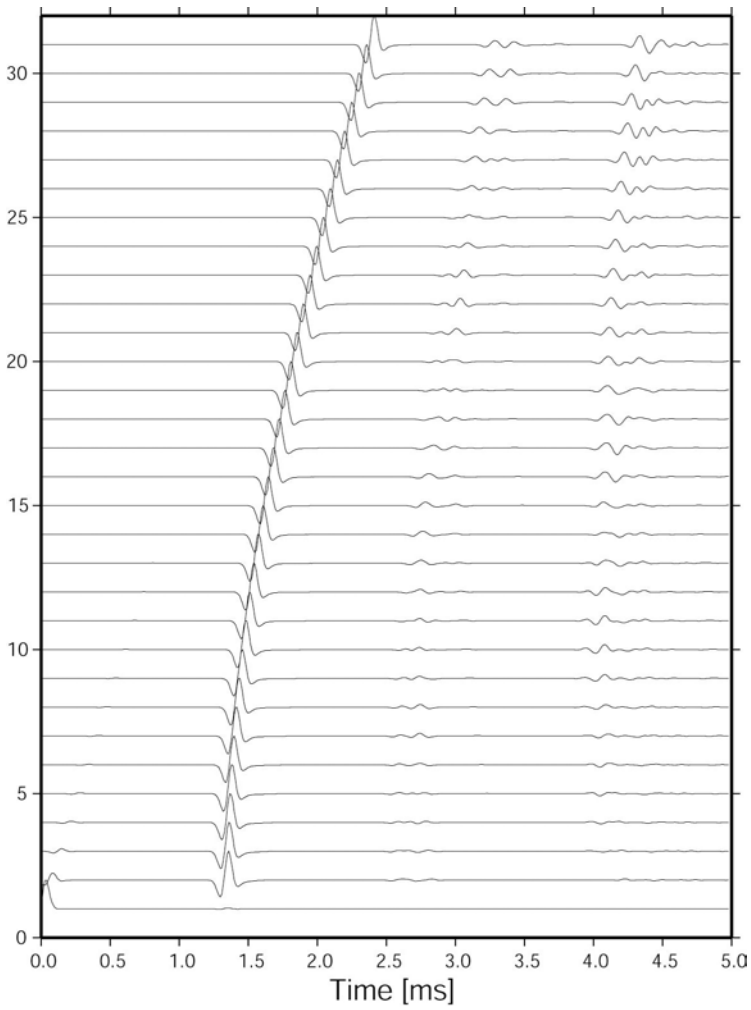

Figure 22: Seismic waveforms generated by the shot at x = 1m and z = 1 m and recorded by the receiver array, calculated for the model in Figure 20 with a free surface boundary condition.

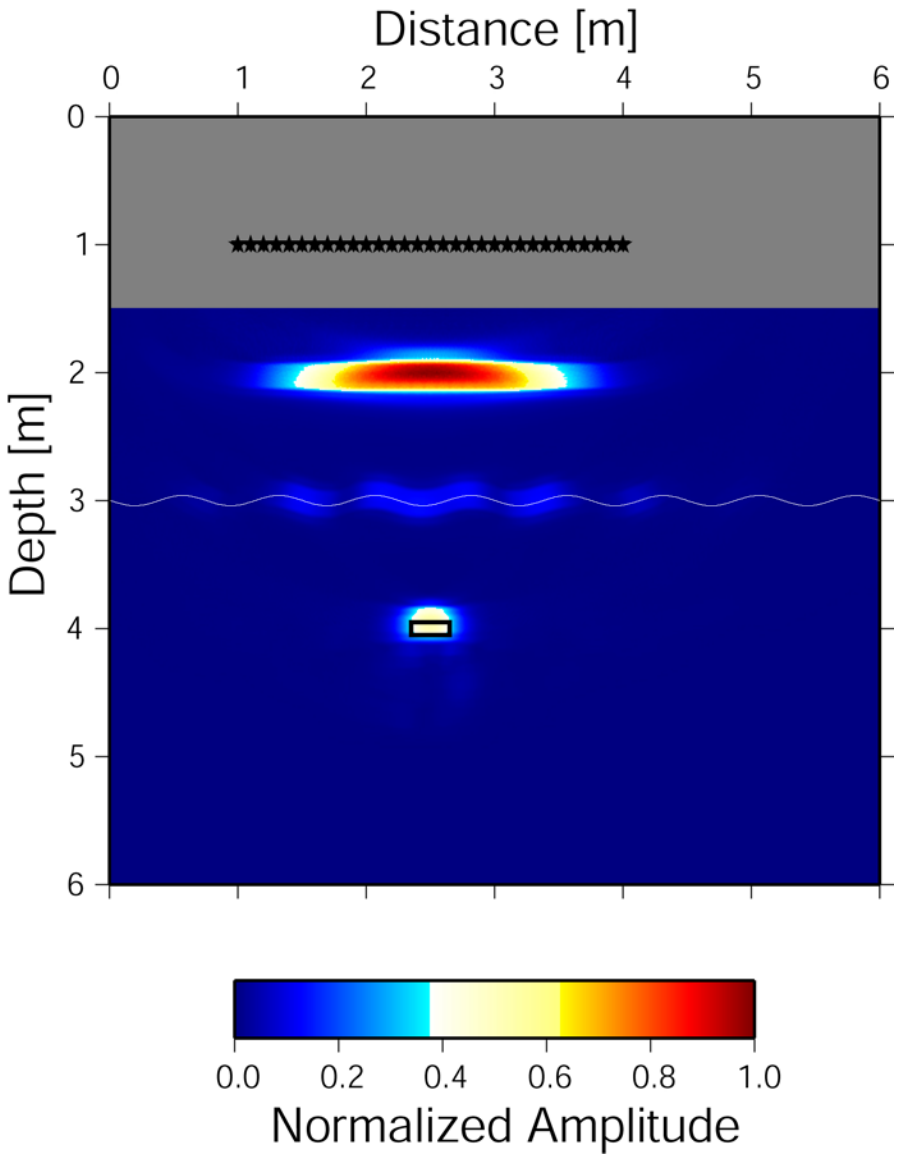

Figure 23: Normalized amplitude map of migrated waveforms recorded by the 31 sources and 31 receivers in the array. The migration was based on a velocity model with a flat seafloor.

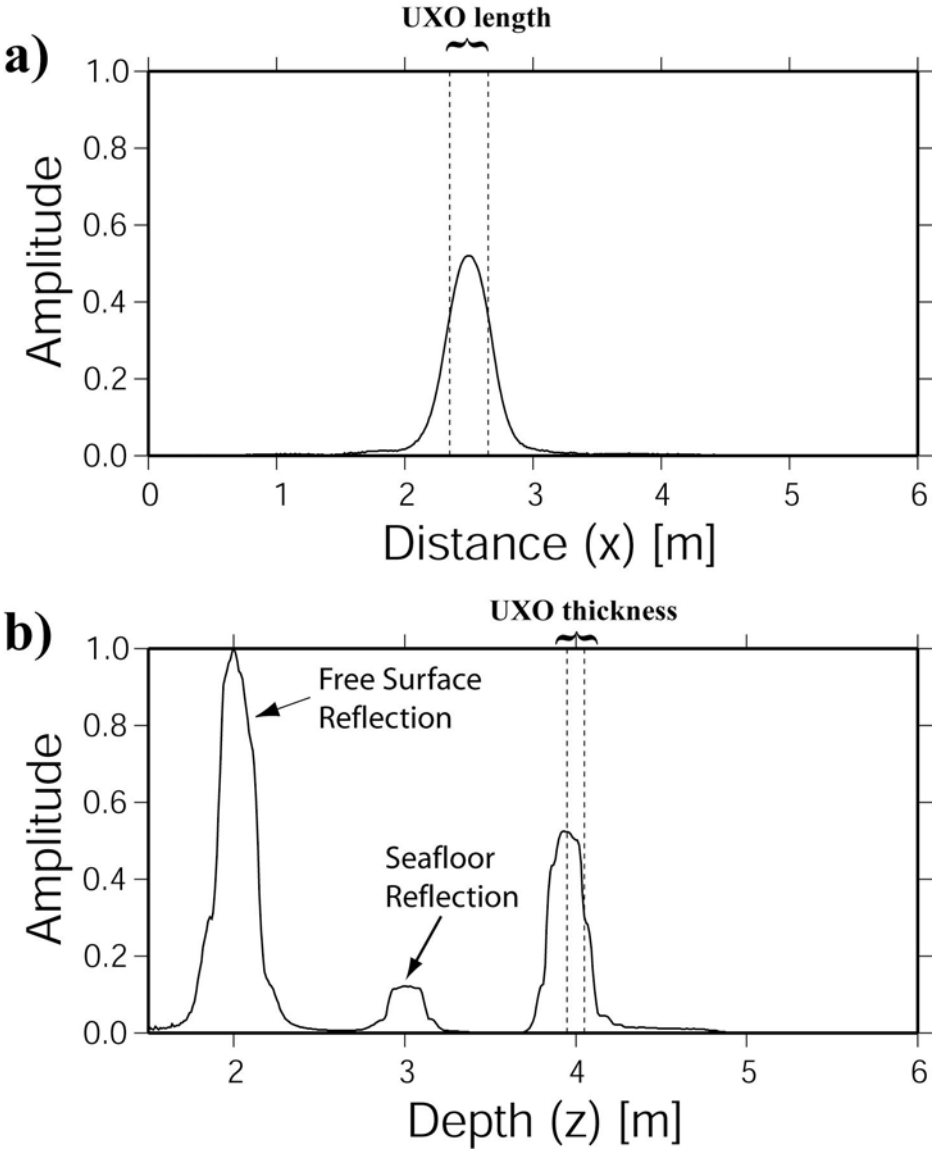

Figure 24: Cross sections of normalized amplitudes through the UXO signature in Figure 23. **a)** Cross section in X-direction. **b)** Cross section in z-direction.

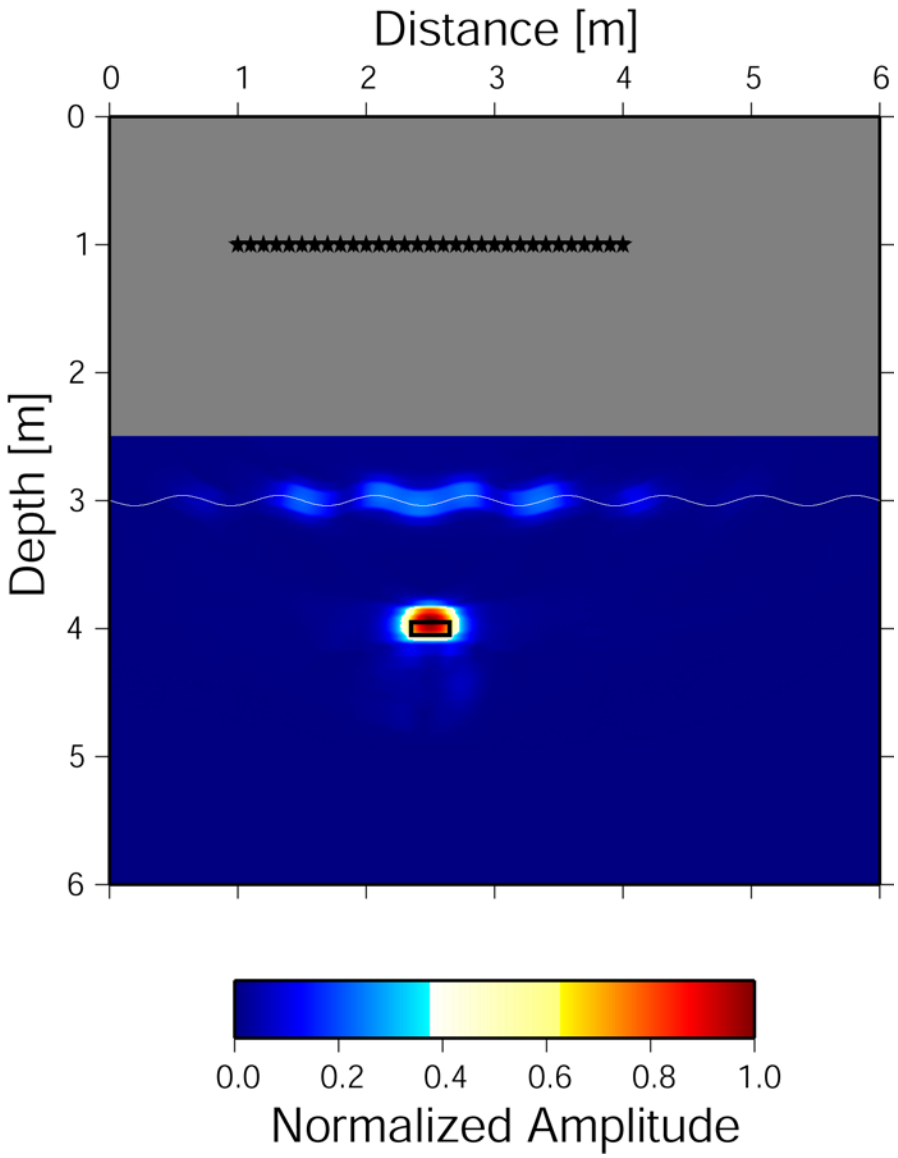

Figure 25: Same as Figure 23 with the exception that the migration was performed between 2.5 m and 6.0 depth.

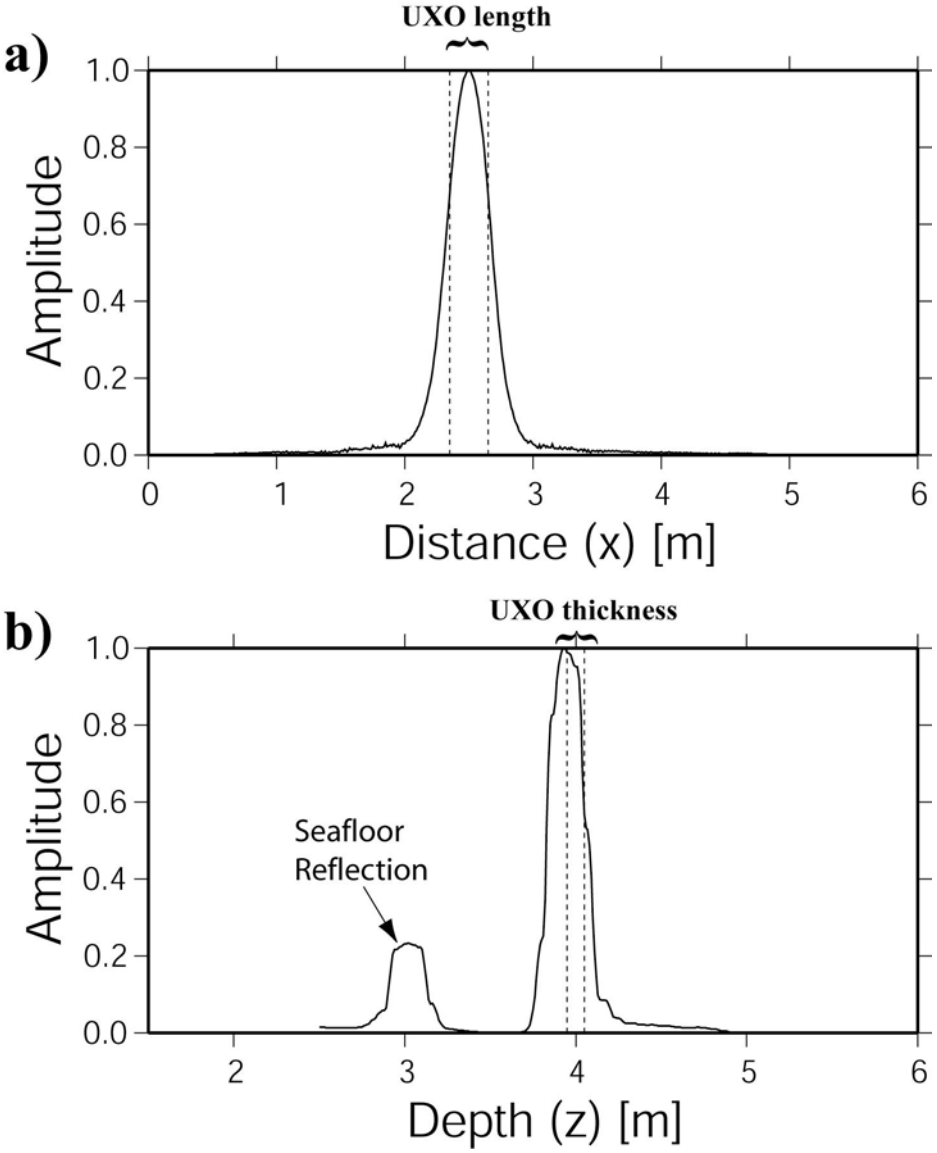

Figure 26: Cross sections of normalized amplitudes through the UXO signature in Figure 25. **a)** Cross section in X-direction. **b)** Cross section in z-direction.

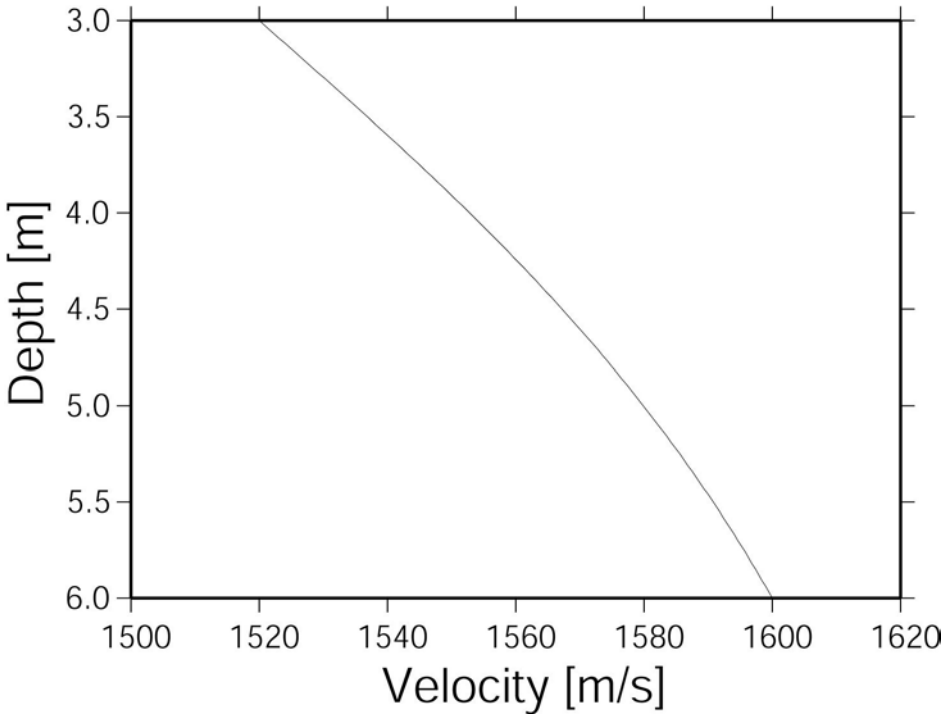

Figure 27: Velocity gradient of the sedimentary layer throughout the finite difference models.

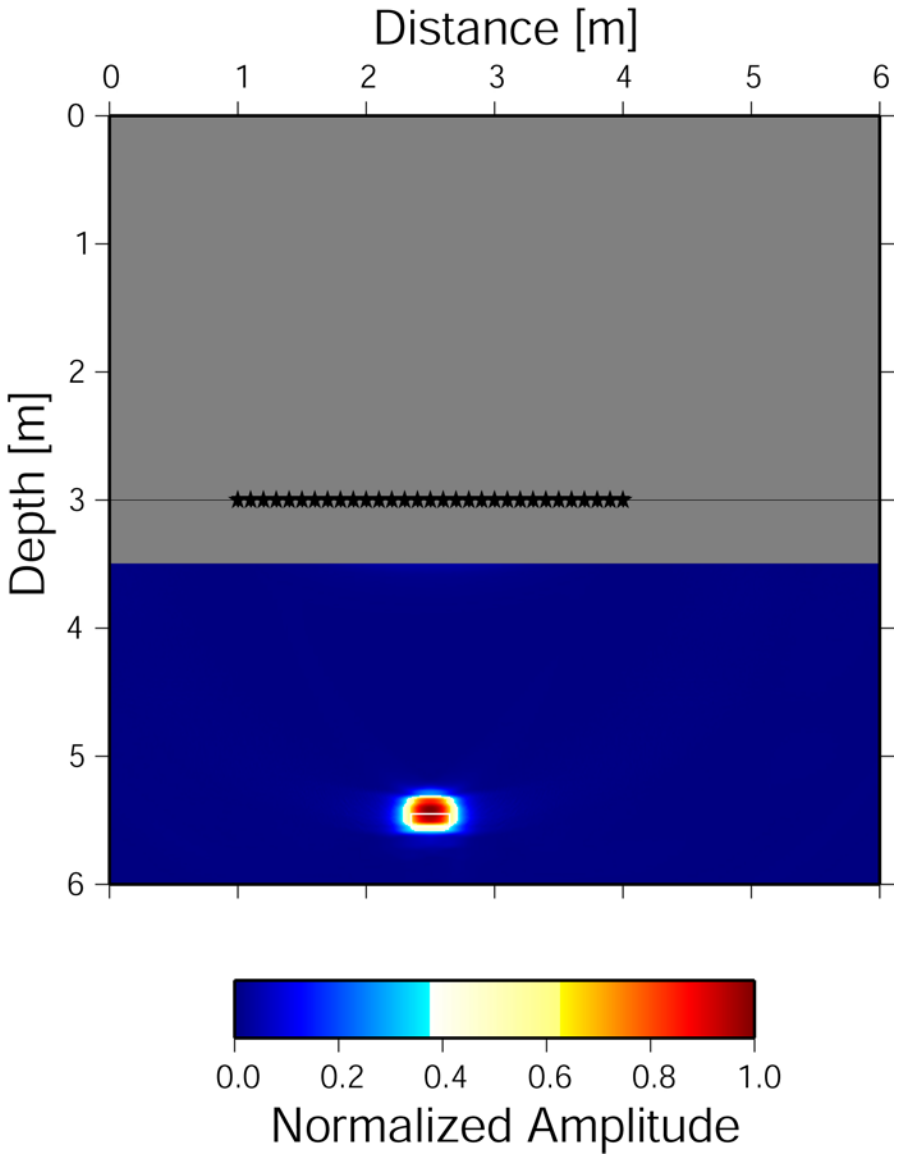

Figure 28: Normalized amplitude map of migrated waveforms recorded by the 31 sources and 31 receivers in the seafloor array for a UXO buried deeper in the sediments.

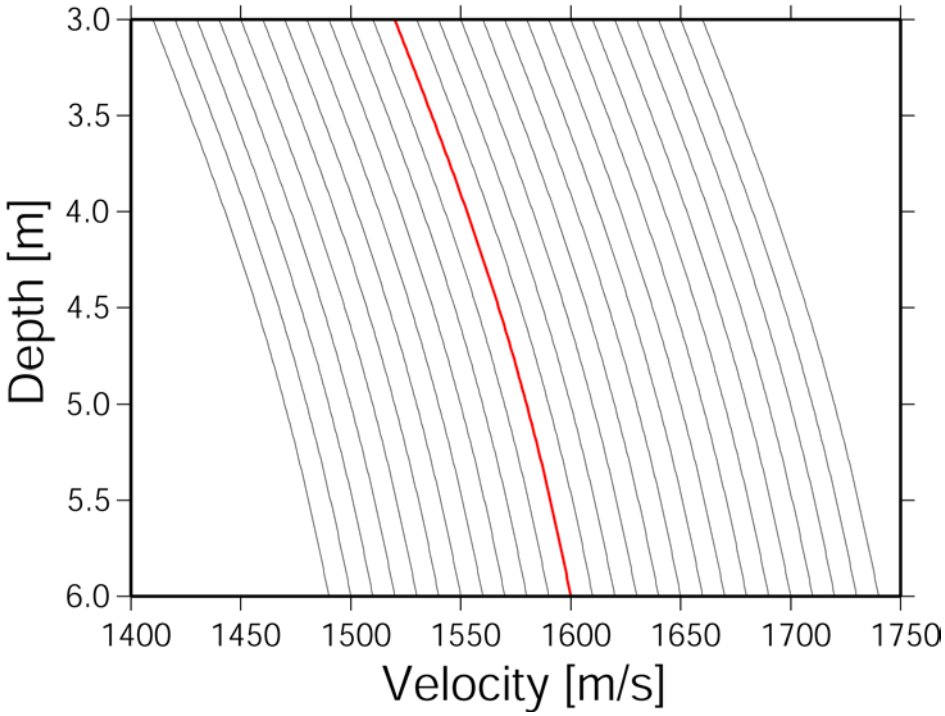

Figure 29: Velocity gradients of the sedimentary layer tested for the best migration result. The red line represents the correct gradient used during the finite difference calculations.

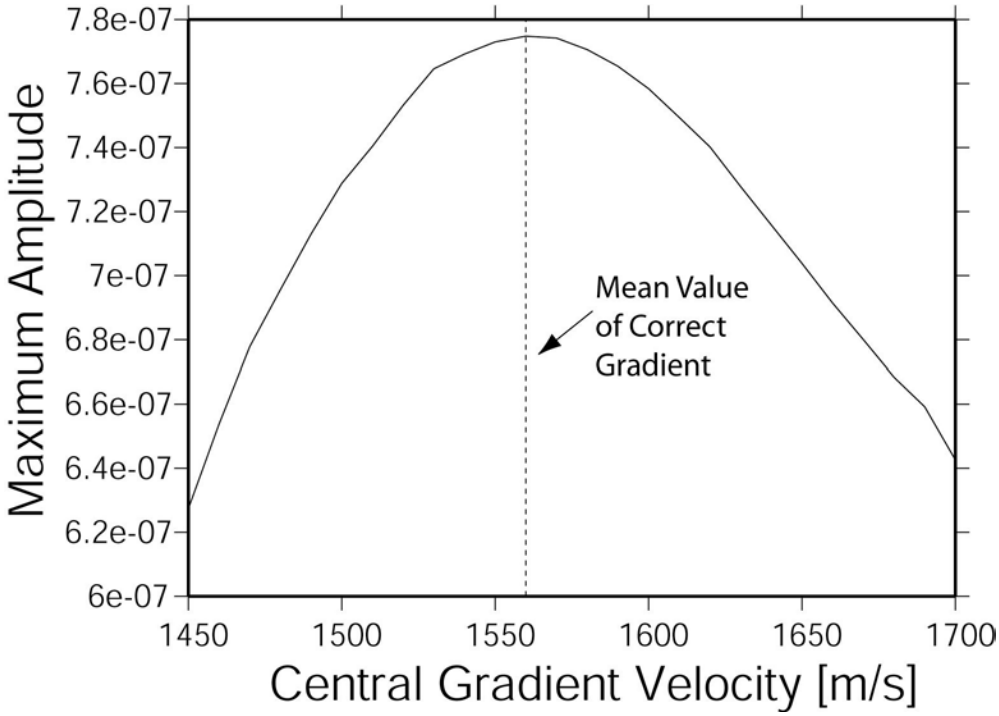

Figure 30: Result of the migration tests based on the velocity gradients in Figure 29. The velocity values on the abscissa are mean values of the end points of each gradient in Figure 29. The dashed line indicates the mean value of the correct gradient.